The antiviral function and regulatory mechanism of linoleic acid against respiratory rhinovirus infection

Kim Taehyun

Department of Medical Science

Graduate School

Yonsei University

The antiviral function and regulatory mechanism of linoleic acid against respiratory rhinovirus infection

Advisor Ryu Ji-Hwan

A Dissertation Submitted
to the Department of Medical Science
and the Committee on Graduate School
of Yonsei University in Partial Fulfillment of the
Requirements for the Degree of
Doctor of Philosophy in Medical Science

Kim Taehyun

June 2025

The antiviral function and regulatory mechanism of linoleic acid against respiratory rhinovirus infection

This Certifies that the Dissertation of Kim Taehyun is Approved

Committee Chair	**Yoon Sang Sun**
Committee Member	**Ryu Ji-Hwan**
Committee Member	**Lee Jae Myun**
Committee Member	**Cho Hyung-Ju**
Committee Member	**Choi Dong Wook**

Department of Medical Science
Graduate School
Yonsei University
June 2025

ACKNOWLEDGEMENTS

First, I would like to express my sincere gratitude to all those who have supported me throughout my doctoral studies. I am deeply thankful to everyone who helped me persevere and continue my academic journey without giving up during this challenging period. Their unwavering encouragement played a crucial role in making this journey possible.

I would like to extend my sincere thanks to the members of my thesis committee: Professor Sang Sun Yoon, Professor Jae Myun Lee, Professor Dong Wook Choi, Professor Hyung-Ju Cho, and my thesis supervisor, Professor Ji-Hwan Ryu. Their invaluable advice and insightful feedback have significantly contributed to the development of this thesis.

I also wish to acknowledge the members of my laboratory for their continuous support, assistance, and collaboration throughout my research. Without their help, this work would not have been possible.

Finally, I would like to express my deepest gratitude to my family and friends for their unconditional support and understanding during this time. Their love and encouragement have been a constant source of strength and motivation.

TABLE OF CONTENTS

LIST OF FIGURES

LIST OF TABLES

ABSTRACT

An antiviral effect of linoleic acid against rhinovirus infection

Human rhinovirus (HRV) infections have been implicated in several respiratory diseases, including common colds, otitis media, sinusitis, exacerbation of asthma, and bronchiolitis. However, there are no specific drugs or vaccines for HRV infection. In this study, I elucidate the protective role of linoleic acid (LA) against HRV infection. It is demonstrated that treatment with LA reduces HRV16 infectivity in human airway epithelial cells. It was uncovered that LA treatment induced the expression of Interferon-stimulated Gene 20 kDa (ISG20), an antiviral protein capable of inhibiting a broad spectrum of viruses, thereby reducing the genomic levels of HRV and capsid proteins. Furthermore, I discovered that the antiviral effect of LA was dependent on G-protein coupled receptor (GPR) 40 and GPR120. Also, LA treatment induce the activation of nuclear factor kappa B (NF-κB) signaling pathways. Using in vivo mouse model, I found intranasal administration of LA attenuated the pathophysiology in HRV-infected mice by inhibiting HRV propagation in a GPR40/120-dependent manner. Collectively, these findings suggest that ISG20 induced by LA treatment inhibits HRV infectivity, and LA may serve as a therapeutic candidate for alleviating various respiratory diseases associated with rhinovirus infection.

Key words : human rhinovirus, linoleic acid, long chain fatty acid, interferon stimulated gene 20kDa, nuclear factor kappa B (NF-κB), G-coupled protein receptor 40/120, antiviral effect.

1. Introduction

Human rhinovirus (HRV) is a positive-sense, single-stranded RNA virus belonging to the genus Enterovirus in the family Picornaviridae. HRV is categorized into three types (A, B and C) based on their specific antigen or genetics. Additionally, HRV is divided into two groups based on the receptor utilization. The common cold is the most characteristic clinical symptom associated with HRV infection, accounting for at least 50% of these cases[1]. HRV infection is associated not only with the development of upper respiratory tract complications such as sinusitis[2] and otitis media[3] but also exacerbations of asthma[4,5], cystic fibrosis[6], and bronchiolitis[7,8] in lower respiratory diseases. However, the development of an HRV vaccine encounters significant challenges due to extensive sequence variations in the antigenic sites[9]. Therefore, investigating treatments for HRV is essential, as there are currently no detailed mechanistic reports or approved antiviral agents available for the prevention or treatment of HRV infection.

Linoleic acid (LA) is classified as a long-chain fatty acid (LCFA) consisting of 18 carbon atoms and two double bonds (18:2) and is recognized as an essential polyunsaturated fatty acid (PUFA) belonging to the omega-6 family. LA cannot be produced by the human body and must be obtained through dietary sources[10,11]. In previous studies, LA has been detected in nasal cavity[12,13] and cholesteryl LA has been associated with antibacterial activity[13]. Recently, it has been reported that LA, which acts through a free fatty acid (FFA)-binding pocket, induces an antiviral effect against severe acute respiratory syndrome coronavirus 2 (SARS-CoV-2). Treatment with LA inhibited viral replication in SARS-CoV-2-infected cells, resulting in fewer deformed virions[14,15]. Additionally, metabolic profiling of the intestines of shrimp infected with white spot syndrome virus (WSSV) confirmed that LA exhibited an antiviral function against WSSV infection[16]. Furthermore, LA, a natural feed compound, has been reported to induce an antiviral effect against porcine epidemic diarrhea virus through the PI3K/AKT/mTOR pathway[17]. Although LA is known to have antiviral effects against various viruses, no study has yet investigated its mechanism of action or its effects on host cells. Furthermore, the effect of LA on HRV infection remains unexplored.

Free fatty acid receptors (FFARs), also known G protein-coupled receptors (GPRs), are activated by free fatty acids[18]. GPR40 (FFAR1), GPR41 (FFAR2), GPR43 (FFAR3), and GPR120 (FFAR4) are representative types of FFARs and have been reported to play various roles in airway epithelial cells. GPR40 regulates tight junction assembly in airway epithelial cells[19]. Activation of GPR41 and GPR43 decreases the expression of tissue plasminogen activator (t-PA) in nasal polyps (NPs), which is correlated with excessive fibrin deposition[20]. Additionally, GPR43 activation alleviates virus-mediated cytotoxicity and promotes antiviral effects via IFN-β against respiratory syncytial virus (RSV) infection[21]. GPR120 activation upregulates IFN-λ in influenza virus infection through IFN regulatory factor (IRF) 1/3[22]. Recently, local administration of acetate, a type of short-chain fatty acid (SCFA), has been shown to augment antiviral effects in vivo[23]. Furthermore, acetate decreases the severity of RSV infection and reduces viral load by modulating the expression of Retinoic acid-inducible gene I (RIG-I)[24]. Although SCFA treatments have demonstrated antiviral effects through FFARs, the relationship between LCFAs, PUFAs and FFARs in HRV infections remains unknown.

Type I IFN, a widely known antiviral innate immune cytokine produced during viral infection, signals through its heterodimeric receptor (IFNAR1/IFNAR2) on airway epithelial cells, activating a set of interferon-stimulated genes (ISGs)[25]. Among these ISGs, ISG20 is a nuclear 3′ −5′ exonuclease that prefers single-stranded RNA (ssRNA)[26]. ISG20 has been shown to restrict the

infection of multiple RNA and DNA viruses[27-29]. A previous study demonstrated that the expression of ISG20 is induced by the nuclear factor kappa B (NF-κB) pathway. Synthetic dsRNA stimulation binds and activates p65 and p50 to the NF-κB element of the ISG20 promoter more rapidly than IFN-induced ISG20 expression, which induces interferon regulatory factor 1 (IRF1) binding to Interferon-sensitive response element (ISRE), thereby inducing a cellular antiviral response to viral infection[30].

In this study, I demonstrated the antiviral function of LA against rhinovirus infection both in vivo and in vitro. I confirmed that the antiviral effect of LA is GPR40/120-dependent, as shown by using specific agonists and antagonists. Furthermore, I identified that NF-κB-ISG20 is the essential pathway in LA-induced HRV inhibition in human airway epithelial cells. This study provides new insights into the antiviral effects of LA against HRV infection and offers potential therapeutic strategies for alleviating diseases caused by rhinovirus.

2. MATERIALS AND METHODS

2.1. Collection of human nasal lavage fluid samples

Human nasal lavage fluids (NLFs) were collected from volunteers, yielding a fixed total volume of 5 ml with saline solution. All samples were promptly centrifuged at 5,000 x *g* for 35 min at 4 °C to eliminate cells and impurities. After centrifugation, the supernatant was carefully collected and filtered using 0.2 μm syringe filters (Sartorius, Göttingen, Germany). Viral RNA was extracted from each sample using the QIAamp viral RNA kits (QIAGEN, Hilden, Germany), according to the manufacturer's instructions. To confirm the presence or absence of human rhinovirus in each sample, one-step RT-qPCR was conducted using human rhinovirus (HRV) specific primers [31]and Luna® Universal Probe One-Step RT-qPCR Kits (NEW ENGLAND Biolabs, Ipswich, MA, USA), according to the manufacturer's instructions. RNA levels were quantified using the HRV specific sequence (HRV forward, 5′- GTG AAG AGC CSC RTG TGC T -3′; HRV reverse, 5′- GCT SCA GG TTA AGG TTA CC -3′; and HRV probe, 5′-(6-FAM™)-TGA GTC CTC CGG CCC CTG AAT G-(TAMRA™)-3′). Subsequently, each sample was classified as the presence or absence of rhinovirus infection and then stored at -80 °C until further analysis. Approval for the study was obtained from the Institutional Review Board (IRB) of Yonsei University College of Medicine (4-2021-0573), with all participants providing informed consent.

2.2. Targeted liquid chromatography-mass spectrometry (LC-MS)

For targeted LC-MS, L-Glutathione reduced (Sigma-Aldrich, St. Louis, MO, USA), N-acetylneuraminic acid (Sigma-Aldrich, St. Louis, MO, USA), Nicotinamide (Sigma-Aldrich, St. Louis, MO, USA), Uric acid (Sigma-Aldrich, St. Louis, MO, USA), Uridine (Sigma-Aldrich, St. Louis, MO, USA), Linoleic acid (Sigma-Aldrich, St. Louis, MO, USA), Linoleic Acid Oxylipins MaxSpec® LC-MS Mixture (Cayman chemical, Ann Arbor, MI, USA), Citric acid (Sigma-Aldrich, St. Louis, MO, USA), L-(+)-Lactic acid (Sigma-Aldrich, St. Louis, MO, USA) and (+) Sodium-L-Ascorbate (Sigma-Aldrich, St. Louis, MO, USA) were used as standard substances. All standards were diluted in distilled water (DW) or ethanol (EtOH) from 1 ppm to 1 ppb for use.

Human NLFs, cell media or mouse bronchoalveolar lavage (BAL) fluids were diluted in methanol (MetOH) by 20 to 200 fold and analyzed on a Thermo Vanquish using the Unison C18 column (3.0 x 150 mm). Each sample was analyzed twice, once in positive and once in negative ion mode. For LC, mobile phase A was 100% water with 0.1% formic acid and mobile phase B was 0.1% formic acid in MetOH : acetonitrile (1:1). The gradient was as follows: 0–0.1 min 10%B, 0.1–2.5 min 1–90%B, 2.5–3 min 90%B, 3–3.1 min 90-5%B, hold 5%B until 5 min. The flow rate was 0.4 ml/min and the column temperature was 45 °C. The injection volume for positive mode was 1 μl. Mass spectrometry was performed with Thermo TSQ Altis. Source parameters were described in Table 1.

Table 1. Mass spectrometry parameters

Description	Parameters
Scan type (m/z)	5-2,000
Sheath gas flow rate (Arb)	50
Aux gas flow rate (Arb)	10
Heater temp (°C)	350
Capillary temp (°C)	325
Spray Voltage (+) (V)	3,500
Spray Voltage (-) (V)	-2,500
RF Lens (V)	49, 52, 57, 70
Normalized collision energy (V)	7-15
Resolution (Full MS)	30,000
Resolution (MS^2)	600

MS: Mass spectrometer

2.3. Cell culture

H1HeLa cells were purchased from American Type Culture Collection (ATCC, Manassas, Virginia, USA) and cultured in Minimum Essential Medium (MEM; Gibco, Waltham, MA, USA) containing 10% (v/v) heat-inactivated fetal bovine serum (FBS; Gibco, Waltham, MA, USA), 1% (v/v) penicillin/streptomycin (Gibco, Waltham, MA, USA). Human lung epithelial cell line BEAS-2B cells were purchased from ATCC. Cells were cultured in RPMI1640 (Gibco, Waltham, MA, USA) containing 10% (v/v) heat-inactivated fetal bovine serum with 1% (v/v) penicillin/streptomycin. Cells were maintained in 175cm^2 flasks (Corning, Tewksbury, MA, USA) at 37 °C in 5% CO_2 incubator. The passage number for all cells used in this study was less than 30.

2.4. Virus infection and metabolite treatment

BEAS-2B cells were seeded 1.5x10^5/well in 12 well plate (Corning, Tewksbury, MA, USA) 24 h prior to infection. The following day, the media was substituted with RPMI1640 containing 2% FBS for virus infection at a multiplicity of Infection (MOI) of 5, and cells were incubated at 33 °C and 5% CO_2 in a humidified incubator for 1 h. After inoculation, cells were washed with PBS and media was substituted with fresh RPMI1640 containing 2% FBS for 24 h. For the metabolite treatment experiments, cells were treated with each concentration of linoleic acid (Sigma-Aldrich, St. Louis, MO, USA), uridine (Sigma-Aldrich, St. Louis, MO, USA), and nicotinamide (Sigma-Aldrich, St. Louis, MO, USA) from 24 h before to 24 h after inoculation. For agonist experiment, 50 μM of GW9508 (MCE, Monmouth Junction, NJ, USA) was treated with the virus for 1 h. To inhibit oxidation of LA, 25 μM of butylated hydroxytoluene (BHT; Sigma-Aldrich, St. Louis, MO, USA) was co-treated with 50 μM of LA. For the LA treatment timing assay, cells were treated with 50 μM LA in RPMI 1640 containing 2% FBS for 24 h prior to HRV16 inoculation, simultaneously during the 1 h HRV16 inoculation, or for 24 h following HRV16 inoculation. To inhibit nuclear factor kappa B (NF-κB), 20 μM caffeic acid phenethyl ester (Sigma-Aldrich, St. Louis, MO, USA) was pre-treated for 30 min, and then washed and treated with LA and virus for 1 h.

2.5. Virus propagation

Human rhinovirus 16 (HRV16; VR-283) and Human rhinovirus 1B (HRV1B; VR-1645) were obtained from ATCC (Manassas, Virginia, USA). For virus propagation, H1HeLa cells were seeded $6x10^6$ in $175cm^2$ flasks (Corning, Tewksbury, MA, USA). The following day, cells were washed with PBS and inoculated with 5 ml of diluted virus stock in serum-free 1x MEM (Gibco, Waltham, MA, USA) at 33 °C and 5% CO_2 in a humidified incubator for 90 min. The flasks were gently rocked every 15 min to distribute the viral inoculum evenly across the monolayer. After inoculation, cells were washed with PBS and the media was substituted with 1x MEM containing 5% FBS. When appropriate cytotoxicity was detected, the flasks were immediately frozen in -80 °C. After freezing and thawing twice, the supernatant was collected and centrifuged at 3,000 x g for 30 min. The supernatant was filtered with 0.2 μm syringe filter (Sartorius, Göttingen ,Germany) and titrated by plaque assay. The supernatant derived from HV1B propagation was concentrated and centrifuged at 2,000 rpm for 2 h using a 100 kDa cutoff filter (Merck Millipore, Darmstadt, Germany).

2.6. Tissue culture infective dose 50% ($TCID_{50}$)

The virus in cell media, mouse lung lysate or mouse BAL fluids was titrated by $TCID_{50}$ method[32,33]. Briefly, H1HeLa cells were seeded $8x10^3$/well in 96 well plate (Corning, Tewksbury, MA, USA). The following day, the virus was serially diluted in 1x MEM containing 1% (v/v) penicillin/streptomycin. Cells were inoculated with serially diluted virus and incubated for 7 days at 33 °C and 5% CO_2 in a humidified incubator. The presence of a cytopathic effect in the wells was used to calculate the $TCID_{50}$ using the Spearman-Karber formula.

2.7. Plaque assay

For plaque assay, H1Hela cells were seeded $5x10^5$/well in 12 well plate (Corning, Tewksbury, MA, USA). The following day, cells were washed with PBS and treated with serially diluted virus. Cells were inoculated with the virus at 33 °C and 5% CO_2 in a humidified incubator for 90 min. After inoculation, cells were washed with PBS and overlaid with plaque assay media (0.5% low-melting agarose (Promega, Madison, WI, USA), 1x MEM containing 2% FBS). The plates were incubated for 5 days at 33 °C and 5% CO_2 in a humidified incubator. Cells were fixed with 4% paraformaldehyde for 1 h and stained with 0.5% crystal violet (Sigma-Aldrich, St. Louis, MO, USA). Viral titers were calculated by counting the plaques and multiplied by dilution factors (Plaque-Forming units/ml).

2.8. Protein quantification by bicinchoninic acid (BCA) assay

Proteins were extracted from BEAS-2B cells and mouse lung tissue using radioimmunoprecipitation assay (RIPA) buffer (Thermo Scientific, Inc, Waltham, MA, USA) with Halt™ Protease & Phosphatase Inhibitor Single-Use Cocktail, EDTA-free (100x) (Thermo Scientific, Inc, Waltham, MA, USA). Total protein concentrations in bronchoalveolar lavage (BAL) fluid, mouse lung lysates, and BEAS-2B cell lysates were measured using the Pierce™ BCA Protein Assay Kit (Thermo Scientific, Inc, Waltham, MA, USA) following the manufacturer's instructions.

Briefly, BAL samples and the albumin standards provided in the kit were incubated with BCA working reagent in a 96-well microplate at 37 °C for 30 min. Absorbance was measured at 562 nm using a VersaMax™ Microplate Reader (Molecular Devices), and protein concentrations were determined based on the standard curve generated from the standards.

2.9. Western blot

Proteins were extracted using radioimmunoprecipitation assay (RIPA) buffer (Thermo Scientific, Inc, Waltham, MA, USA) with Halt™ Protease & Phosphatase Inhibitor Single-Use Cocktail, EDTA-free (100x) (Thermo Scientific, Inc, Waltham, MA, USA). Equal amounts of proteins (15 μg) were separated by 10% SDS-PAGE gels and transferred to polyvinylidene difluoride (PVDF) membranes (Merck Millipore, Darmstadt, Germany). After transfer, membranes were blocked with 5% skim milk in TTBS for 1h in room temperature. Membranes were incubated with primary antibodies in 5% skim milk with TTBS at 4 °C overnight. The following day, membranes were washed three times with TTBS and incubated with secondary antibodies in 5% skim milk with TTBS for 1 h in room temperature. Blots were visualized using Pierce ECL Western Blotting Substrate (Thermo Scientific, Inc, Waltham, MA, USA) and exposed to X-ray film. The list of antibodies used in immunoblotting includes: mouse anti-Human Rhinovirus antibody (QED Bioscience, San Diego, CA, USA), rabbit anti-phospho-NF-κB p65 antibody (Cell Signaling Technology, Danvers, MA, USA), rabbit anti-NF-κB p65 antibody (Cell Signaling Technology, Danvers, MA, USA), mouse anti-GAPDH antibody (Santa Cruz, Dallas, Texas, USA), rabbit anti-ISG20 antibody (Invitrogen, Carlsbad, CA, USA) for primary antibodies, and goat anti-mouse IgG (H+L)-HRP (GenDEPOT, Barker, Texas, USA) and goat anti-rabbit IgG (H+L)-HRP (Jackson ImmunoResearch Laboratory, West Grove, Pensylvania, USA) for secondary antibodies.

2.10. Real-time quantitative polymerase chain reaction (RT-qPCR)

Total RNA was isolated from BEAS-2B cells or mouse lung lysates using Hybrid-R™ (GeneAll Biotechnology Co., Ltd, Seoul, Republic of Korea). Complementary DNA (cDNA) was synthesized from 500 ng of RNA with random hexamer primers (Invitrogen, Carlsbad, CA, USA), RNase inhibitor (Applied Biosystems, Foster City, CA, USA), dNTPs (Applied Biosystems, Foster City, CA, USA), and M-MLV reverse transcriptase (Invitrogen, Carlsbad, CA, USA). For quantitative PCR (qPCR), KAPA SYBR FAST qPCR master mix (2X) (Roche, Basel, Switzerland) was used according to the manufacturer's instructions. qPCR was performed using QuantStudio 3 Real-Time PCR System (Thermo Scientific, Inc, Waltham, MA, USA). Gene expression levels were evaluated using the comparative Ct method (2-ΔΔCt method). Primers used for real-time qPCR in this study are listed in Table 2.

Table 2. Primer sequences for RT-qPCR

Target	Gene Sequence
Human 18s rRNA	F: 5'-GCT TAA TTT GAC TCA ACA CGG GA-3'
	R: 5'-AGC TAT CAA TCT GCT AAT CCT GTC-3'
HRV16	F: 5'-TCT CTA CAG GGC CCT TAC TCG-3'
	R: 5'-CCA CTC TTC TCT CGG GAA CTT-3'
HRV1B	F: 5'-CCA TCG CTC ACT ATT CAG CAC-3'
	R: 5'- TCT ATC CCG AAC ACA CTG TCC-3'
Human ISG20	F: 5'-AGC GGC TAC ACA ATC TAC GA-3'
	R: 5'- AGG CTG TTC TGG ATG CTC TT-3'
Human DMBT1	F: 5'- ACT ACG ACA GAT TGG TGG CA-3'
	R: 5'- GTT GGG GTA GTA TGC AGG GT-3'
Human TRIM35	F: 5'- GCT TCG CGA GTT CTT GAG AG-3'
	R: 5'- GCT GCT TCA TCT TCT CGT CG-3'
Human TRIM27	F: 5'- TGT TTG GGA GTT TGA GCA GC-3'
	R: 5'- AAG AGA ACT GGG TGA TGG CA-3'
Human IRF1	F: 5'- AGG GGA AAA GGA GCC AGA TC-3'
	R: 5'- CCT TGT TCC TGC TCT GGT CT-3'
Murine Gapdh	F: 5'-AAC GAC CCC TTC ATT GAC CT-3'
	R: 5'-TGG AAG ATG GTG ATG GGC TT-3'
Murine Il6	F: 5'-AGA CTT CCA TCC AGT TGC CT-3'
	R: 5'-CAG GTC TGT TGG GAG TGG TA-3'

2.11. Lactate dehydrogenase (LDH) assay

Cell cytotoxicity was measured using CytoTox 96 Non-Radioactive Cytotoxicity Assay kit (Promega, Madison, WI, USA) according to the manufacturer's instructions. Briefly, culture supernatants of BEAS-2B cells were collected and incubated with the reagent for 30 min in a 96-well plate (SPL life science, Pocheon, Republic of Korea). After incubation, the results were obtained at 490 nm using a spectrophotometer. Positive control was supplied with the kit and the culture media was used as the negative control.

2.12. Bulk mRNA sequencing and data analysis

Total RNA was isolated from BEAS-2B cells using Hybrid-R™ (GeneAll Biotechnology Co., Ltd., Seoul, Republic of Korea). Total RNA concentration was calculated by Quant-IT RiboGreen (Invitrogen, Carlsbad, CA, USA). To assess the integrity of the total RNA, samples are run on the TapeStation RNA screentape (Agilent Technologies, Santa Clara, CA, USA). Only high-quality RNA preparations, with RIN greater than 7.0, were used for RNA library construction. A library

was independently prepared with 1 μg of total RNA for each sample by Illumina TruSeq Stranded mRNA Sample Prep Kit (Illumina, Inc., San Diego, CA, USA). The first step in the workflow involves purifying the poly-A containing mRNA molecules using poly-T-attached magnetic beads. Following purification, the mRNA is fragmented into small pieces using divalent cations under elevated temperature. The cleaved RNA fragments are copied into first strand cDNA using SuperScript II reverse transcriptase (Invitrogen, Carlsbad, CA, USA) and random primers. This is followed by second strand cDNA synthesis using DNA Polymerase I, RNase H and dUTP. These cDNA fragments then go through an end repair process, the addition of a single 'A' base, and then ligation of the adapters. The products are then purified and enriched with PCR to create the final cDNA library. The libraries were quantified using KAPA Library Quantification kits for Illumina Sequencing platforms according to the qPCR Quantification Protocol Guide (Kapa Biosystems, Inc., Wilmington, MA, USA) and qualified using the TapeStation D1000 ScreenTape (Agilent Technologies, Santa Clara, CA, USA). Indexed libraries were then submitted to an Illumina NovaSeqX (Illumina, Inc., San Diego, CA, USA), and the paired-end (2×100 bp) sequencing was performed by the Macrogen Incorporated.

RNA sequencing reads were aligned to the reference genome GRCh38 with the STAR aligner (version 2.5.4b). For the batch correction, ComBat-seq function in the Bioconductor package sva (version 3.54.0) was used. The Bioconductor DEseq2 package (version 1.44.0)[34] was used to perform differential gene expression analysis. Gene count data was imported and normalized using the DESeq2 default normalization methods. Gene Set Enrichment Analysis (GSEA) was conducted using the GSEA module on the GenePattern public server (https://cloud.genepattern.org)[35,36]. C5 gene sets containing the gene ontology (GO) gene sets from the MSigDB collections (version 2024.1) were used with the default settings of the GSEA module.

2.13. Enzyme-linked immunosorbent assay (ELISA)

The supernatants of BEAS-2B cells were collected at 24 hpi and stored at −80 °C. For mouse bronchoalveolar lavage (BAL) fluid, samples were collected by washing the lungs with 1 ml of ice-cold PBS at 8 hpi. After centrifugation at 1700 × g for 5 min, the supernatants were collected and stored at −80 °C until further use. Levels of human IFN-β (R&D systems, Minneapolis, MN, USA) in cell media, as well as mouse IL-6 (R&D systems, Minneapolis, MN, USA), mouse IFN-β (R&D systems, Minneapolis, MN, USA) and mouse IL-28A/B (IFN-lambda 2/3; R&D systems, Minneapolis, MN, USA) in mouse BAL fluid, were quantified using the corresponding DuoSet® ELISA kits according to the manufacturer's instructions. The absorbance was measured at 450 nm using a VersaMax™ Microplate Reader (Molecular Devices, Sunnyvale, CA, USA). The data were analyzed with SoftMax® Pro Software v5.2 (Molecular Devices, Sunnyvale, CA, USA).

2.14. Short hairpin RNA (shRNA) transfection with lentivirus

For the knock-down of human ISG20, Lentivirus starter kit was purchased from Lugen Sci (Seoul, Repulic of Korea) and followed by manufacturer's instructions. Briefly, BEAS-2B cells were seeded $1x10^5$/well in 12 well plate prior to lentivirus infection. The following day, BEAS-2B cells were washed with PBS transfected with lentiviral shRNAs (MOI 20) using 1 X Lenti-TD-MAX (Lugen Sci Co., Ltd, Seoul, Republic of Korea). After 24 h inoculation, cells were washed with PBS and constituted with fresh culture media containing 1 μM puromycin

(Invivogen, San Diego, CA, USA) for positive selection. All knockdown cells used in this study were validated by the ISG20 expression by RT-qPCR and western blot. The sequence for the ISG20-specific shRNA was 5'-GAC ATG AGC GGC TAC ACA ATC-3'. For scrambled shRNA 5'-GCA CTA CCA GAG CTA ACT CAG ATA GTA CT-3' was used.

2.15. In-vivo mouse model and histological analysis

6 weeks-old female Balb/c mice were purchased from Orient Bio Inc. (Sungnam, Republic of Korea). All mice used in this study were maintained in Animal Biosafety Level 2 (ABSL-2) facility. All animal work was approved by the Institutional Animal Care and Use Committee (IACUC) at Yonsei University College of Medicine (protocol number 2022-0282), according to guidelines outlined by the Association for Assessment and Accreditation of Laboratory Animal Care (AAALAC) International (facility number 001071). Balb/c mice were intranasally inoculated with 5 x 10^6 $TCID_{50}$ (50 μl) of HRV1B. To inactivate HRV1B, it was exposed to 1,200 mJ/cm^2 of UV light for 30 min. For local administration of LCFAs, linoleic acid sodium salt (2.5 mg/kg), oleic acid sodium salt (2.5 mg/kg), palmitic acid sodium salt (2.5 mg/kg), or palmitoleic acid sodium salt (2.5 mg/kg) (all from Sigma-Aldrich, St. Louis, MO, USA) was intranasally co-administered with HRV1B. For inactivation of GPR120 and GPR40, Balb/c mice were intraperitoneally injected GPR120 antagonist (AH7614; MCE, Monmouth Junction, NJ, USA, 2.5mg/kg) and GPR40 antagonist (GW1100; MCE, Monmouth Junction, NJ, USA, 2.5mg/kg) 30 min before HRV1B infection. BAL fluid was collected by flushing with ice-cold PBS through a catheter (BD Biosciences, San Jose, CA, USA). For histological analysis, lung tissues were collected from mice at 16 hpi after whole-body perfusion. The tissues were fixed in 4% PFA for 24 h and embedded in paraffin. Tissue sections were stained with hematoxylin and eosin (H&E) to evaluate inflammatory cell infiltration. Lung injury was assessed as described previously[37]. Briefly, lung sections stained with H&E were scored by blinded reviewers for the presence and severity of inflammation. The extent of perivascular and peribronchial infiltrates, edema, alveolar septal infiltrates, hemorrhage, and epithelial damage were evaluated using the following scoring system: 0, absence; 1, mild; 2, moderate; and 3, severe.

3. Results

3.1. Metabolite profiles in human nasal lavage fluid are correlated with the presence of rhinovirus

Previous literature indicated that several metabolites are related with antiviral effects against viral infection [38-41]. Based on previously published literature, 9 potential metabolites were selected, including linoleic acid (LA), uridine, nicotinamide, uric acid, ascorbic acid, lactic acid, citric acid, N-acetylneuraminic acid, and glutathione, which have the potential to suppress human rhinovirus (HRV) infection [38,40-49]. To identify the potential metabolite candidates, human nasal lavage fluids (NLFs) from volunteers were obtained (Table 3). Samples were determined by one-step qPCR and conducted targeted LC-MS/MS-based metabolomics (Figure 1). Through one-step qPCR, the 5'-UTR of HRV gene was detected in the HRV-positive group, but was not detected in the HRV-negative group (Figure 2). Next, NLFs were conducted targeted LC-MS/MS-based metabolomics analysis (Figure 1). Interestingly, LC-MS/MS analysis revealed the quantity of metabolites such as LA, uridine, and nicotinamide was increased in HRV-positive human NLFs, compared to HRV-negative human NLFs (Figure 3A-C). However, no differences were observed in the other metabolites in human NLFs (Figure 3D-I). These results collectively indicate that the concentration of certain metabolites in NLFs is associated with the presence of HRV.

Table 3. Description of nasal lavage fluid volunteers (*n* = 15)

Sex	Blood type	Diagnosis	Allergy	Smoking	HRV
M	B+	Chronic sinusitis with nasal polyp	+	Ex-smoker	-
M	B+	Septal deviation	+	Non smoker	-
F	O+	Chronic sinusitis with nasal polyp	+	Non smoker	-
F	O+	Chronic sinusitis with nasal polyp	-	Non smoker	-
M	O+	Septal deviation	+	Current smoker	-
F	A+	Chronic sinusitis	-	Non smoker	-
F	A+	Septal deviation	-	Non smoker	-
M	B+	Chronic sinusitis	-	Non smoker	-
F	A+	Septal deviation	+	Non smoker	-
M	B+	Septal deviation	+	Non smoker	+
F	B+	Chronic sinusitis with nasal polyp	-	Non smoker	+
F	O+	Chronic sinusitis with nasal polyp	+	Non smoker	+
M	B+	Septal deviation	+	Non smoker	+
F	O+	Nasolabial cyst	+	Non smoker	+
F	A+	Chronic sinusitis with nasal polyp	+	Non smoker	+

M: Male; F: Female; -: negative; +: positive

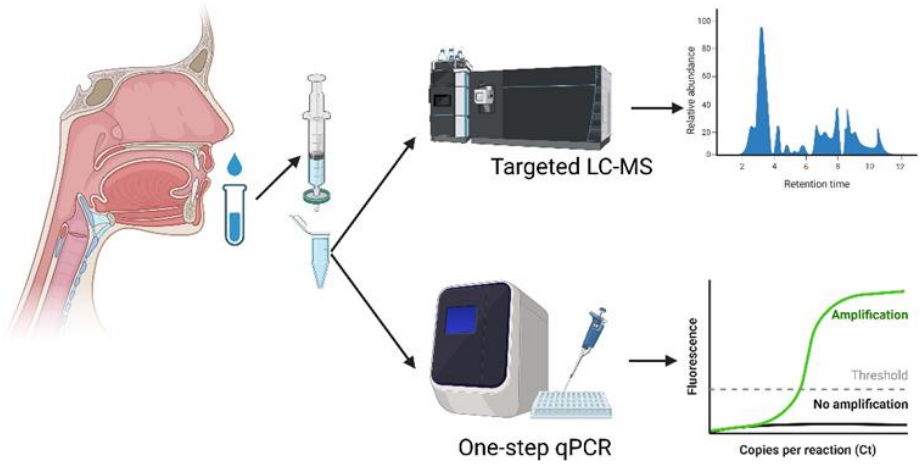

Figure 1. A schematic illustration of metabolite detection using human nasal lavage fluids. A schematic illustration of metabolite detection using human nasal lavage fluids (NLFs) is presented. Human NLFs were collected from volunteers, with samples categorized as HRV-positive (+) or HRV-negative (-) through one-step qPCR (n = 9 for HRV(-), n = 6 for HRV(+)). Each human NLF sample was subsequently analyzed using LC-MS/MS-based targeted metabolomics.

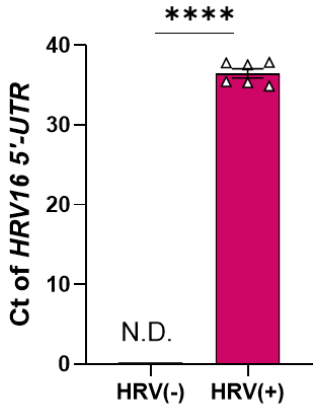

Figure 2. Human rhinovirus (HRV) detected in human nasal lavage fluid samples. The HRV 5'-UTR gene was measured by one-step qPCR in NLFs from volunteers. The threshold cycle (Ct) values for HRV 5'-UTR were used to diagnose HRV infection. Data are presented for HRV-negative (HRV(-), $n = 9$) and HRV-positive (HRV(+), $n = 6$) groups. Results are shown as the mean ± SEM; *$p < 0.05$; **$p < 0.01$; ***$p < 0.001$; ****$p < 0.0001$ using Student's t-test.

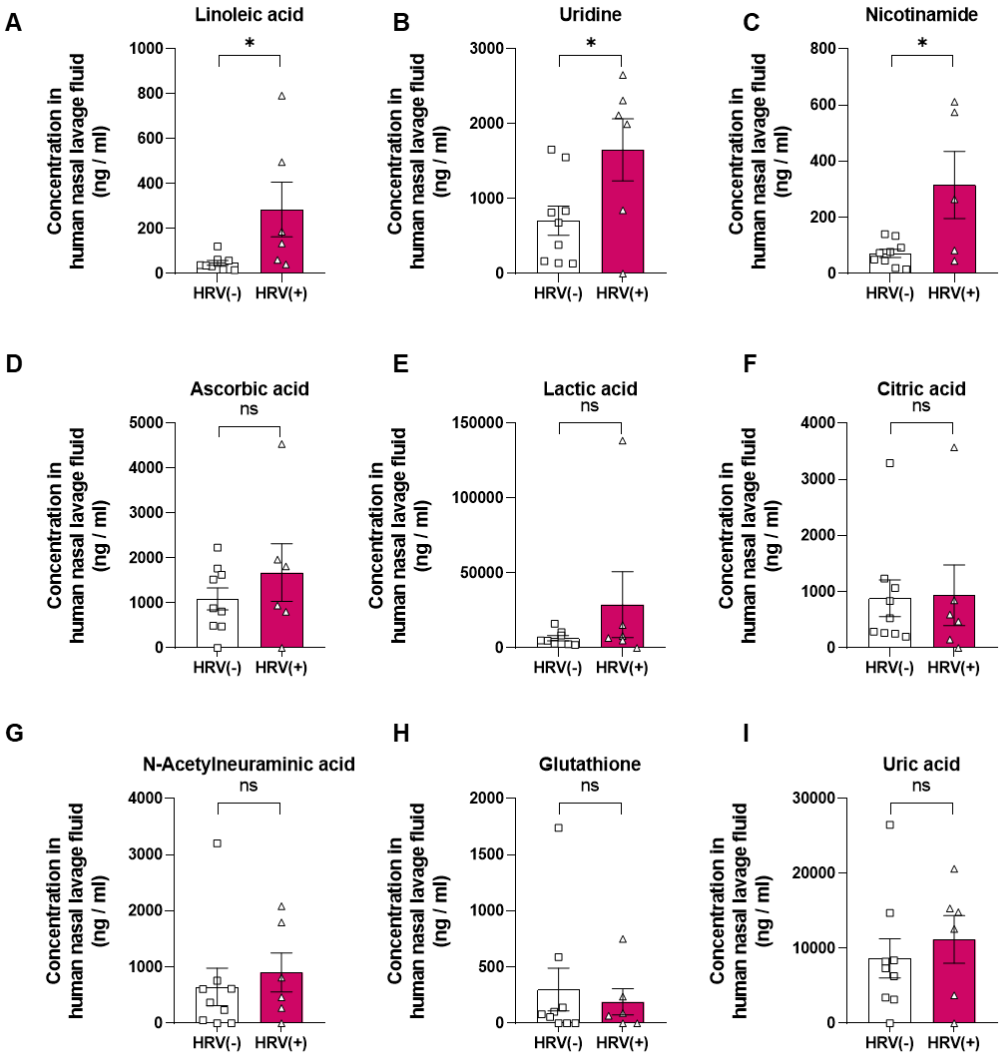

Figure 3. Metabolite profiles in human NLFs are correlated with the presence of HRV. Quantification of metabolite concentrations in human NLFs. NLFs were analyzed by LC-MS/MS-based targeted metabolomics analysis (n = 9 for HRV (-), n = 6 for HRV (+)). Concentration of (A) linoleic acid, (B) uridine, (C) nicotinamide, (D) ascorbic acid, (E) lactic acid, (F) citric acid, (G) N-acetylneuraminic acid, (H) glutathione, (I) uric acid were analyzed using LC-MS/MS-based targeted metabolomics (n = 9 for HRV(-), n = 6 for HRV(+)). Results are shown as the mean ± SEM; *p < 0.05; **p < 0.01; ***p < 0.001; ****p < 0.0001 using Student's t-test.

3.2. Treatment with LA reduces HRV16 infection in BEAS-2B cells

To elucidate the properties of metabolites in human NLFs against HRV infection, HRV16 was infected multiplicity of infection (MOI) 5 in the human lung epithelial cell line, BEAS-2B cells (Figure 4A). Compared to the control media, HRV16 mRNA expression levels were significantly increased at 16 hpi, peaking at 24 hpi (Figure 4B). Subsequently, HRV16 mRNA expression levels progressively were decreased and not detected at 48 hpi (Figure 4B). To identify the antiviral effect of LA, uridine, and nicotinamide, which were significantly elevated in HRV-positive human NLFs (Figure 3A-C), these metabolites were treated with HRV16 in BEAS-2B cells (Figure 5A). Interestingly, LA significantly decreased HRV16 mRNA expression levels in dose-dependent manner at 24 hpi (Figure 5B). However, uridine and nicotinamide showed no effect at 24 hpi (Figure 5B). Treatment with each metabolite had no effect on cell cytotoxicity (Figure 5C). Since only LA exhibited the antiviral effect against HRV16 infection, LA was selected as a potential target for future investigation. In line with the effect of LA on HRV16 mRNA expression levels, treatment with LA also decreased HRV16 capsid proteins, VP0 and VP2 in cell lysate (Figure 5D) and virus titer in cell media at 24 hpi (Figure 5E). Next, I conducted an experiment to determine whether the timing of LA treatment influenced the antiviral effect (Figure 6A). Notably, LA treatment suppressed viral gene expression regardless of whether it was applied prior to, during, or after viral infection (Figure 6B), suggesting that LA exerts its antiviral effect intracellularly.

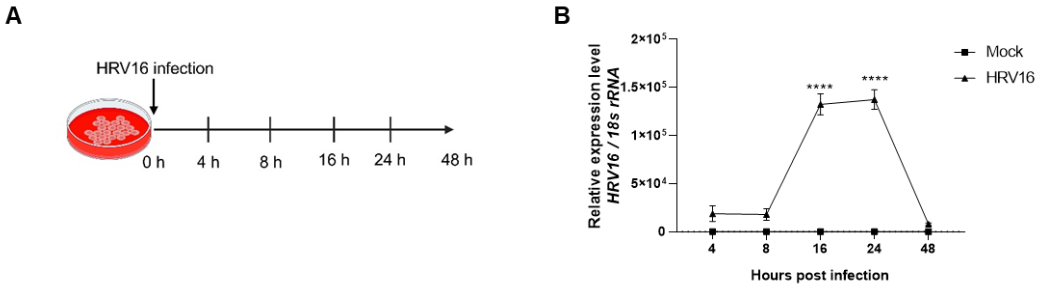

Figure 4. Kinetics of HRV16 infection in BEAS-2B cells. (A) Schematic illustration of in vitro experiment using BEAS-2B cells. (B) Time-course analysis of HRV16 mRNA expression in BEAS-2B cells was performed by qPCR to assess the infection dynamics (n = 4). Results are shown as the mean ± SEM; *p < 0.05; **p < 0.01; ***p < 0.001; ****p < 0.0001 using two-way ANOVA with Sidak's multiple comparison test.

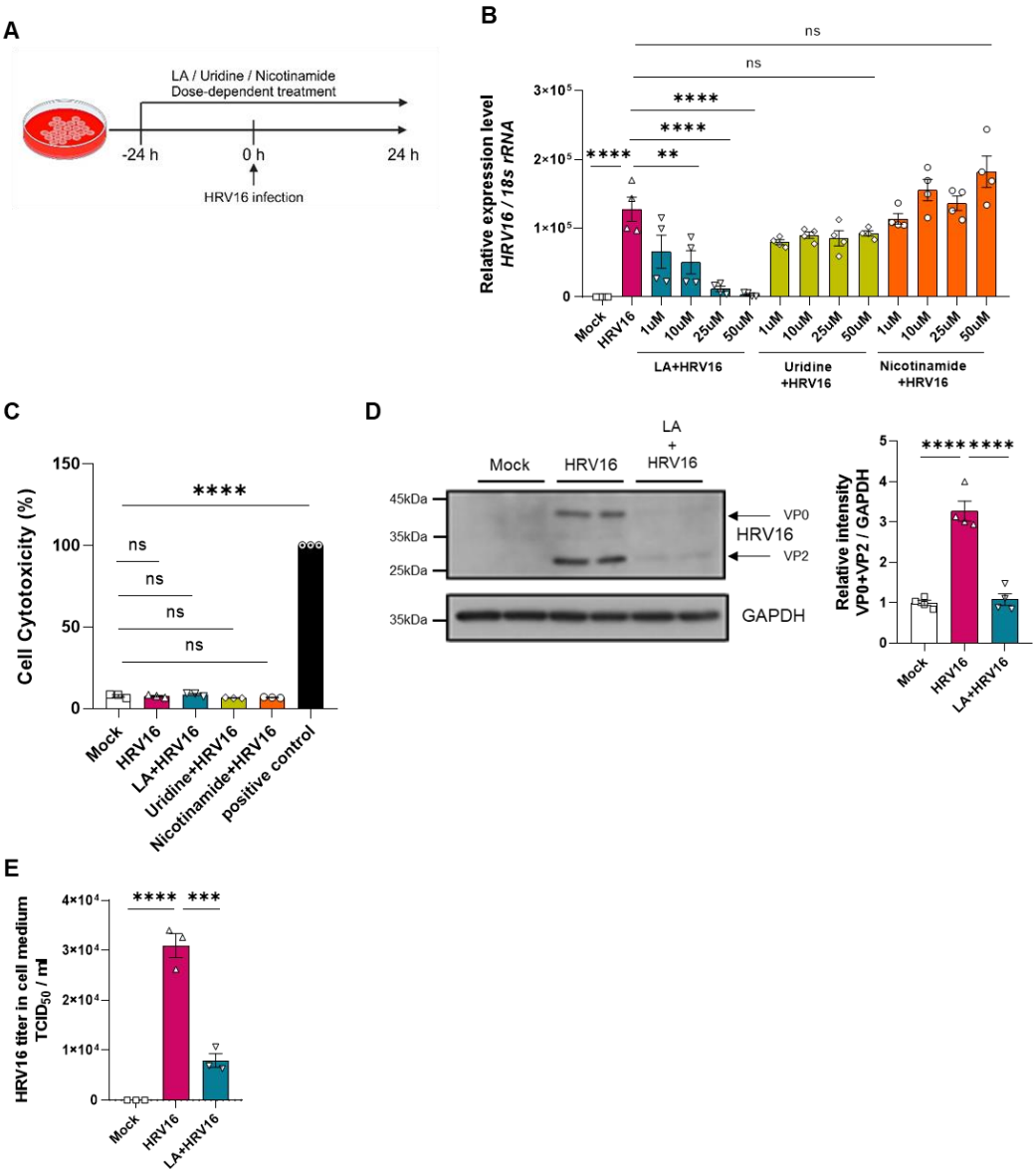

Figure 5. Treatment of LA reduces HRV16 infection in BEAS-2B cells. (A) Schematic illustration of metabolite treatment experiment using BEAS-2B cells. (B) Relative HRV16 mRNA expression levels in each metabolite-treated BEAS-2B cells were measured by qPCR at 24 hpi (n = 4). Concentration of LA (1, 10, 25, 50 μM), Uridine (1, 10, 25, 50 μM), and Nicotinamide (1, 10, 25, 50 μM). (C) Cell cytotoxicity in metabolite-treated (50 μM) BEAS-2B cell media was measured by an LDH assay at 24 hpi (n = 3). (D) Representative immunoblot analysis of HRV16 capsid proteins (VP0, VP2) in Mock, HRV16, and LA (50 μM) + HRV16 treated BEAS-2B cell lysates at 24 hpi (n = 4). Relative intensity of viral protein levels was quantified with image J. The intensity of VP0, VP2 proteins was normalized with GAPDH. (E) Viral load in HRV16 infected BEAS-2B cells was measured by $TCID_{50}$ in the culture supernatant (n = 3). Results are shown as the mean ± SEM; *$p < 0.05$; **$p < 0.01$; ***$p < 0.001$; ****$p < 0.0001$ using one-way ANOVA with Tukey's multiple comparisons test.

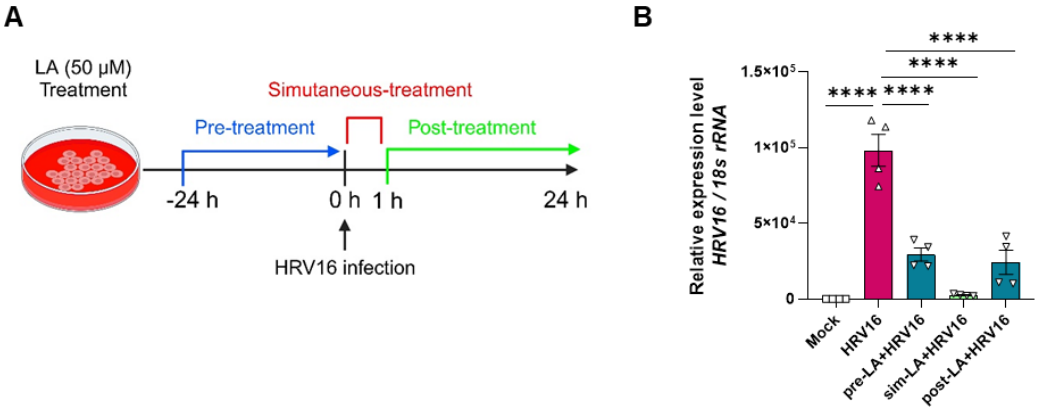

Figure 6. LA reduces HRV16 replication in BEAS-2B cells regardless of treatment timing. (A) Schematic illustration of the experimental design evaluating different LA treatment timings in BEAS-2B cells. (B) Relative HRV16 mRNA expression levels in Mock, HRV16, and HRV16+LA (50 μM) treatments, including pre-treatment (pre-LA + HRV16; 24 h before HRV16 infection), simultaneous-treatment (sim-LA + HRV16; 1 h with HRV16 infection), and post-treatment (post-LA + HRV16; 1 h after HRV16 infection) (n = 4). Results are shown as the mean ± SEM; *p < 0.05; **p < 0.01; ***p < 0.001; ****p < 0.0001 using one-way ANOVA with Tukey's multiple comparisons test.

3.3. LA exhibits antiviral effect regardless of its oxidation

A previous study has shown that LA undergoes oxidative degradation within approximately 40 hours under oxidative conditions. Through this process, LA generates various oxylipins, including hydroxy-octadecadienoic acids (HODEs), oxo-octadecadienoic acid (Oxo-ODEs), epoxyoctadecenoic acids (EpOMEs), and dihydroxyoctadecenoic acids (DiHOMEs) [50]. Recently, 18-hydroxy eicosapentaenoic acid (18-HEPE), an oxidative form of ω-3 fatty acid, induced by *Clostridium butyricum*, was found to promote IFN-λ production [22], suggesting that oxidized forms of LA may influence antiviral activity.

To directly assess the extent of LA oxidation, targeted LC-MS analysis was performed on the culture media under three conditions: media only, media containing LA, and media containing both LA and butylated hydroxytoluene (BHT, 25 μM), a known antioxidant [51].

LC-MS analysis revealed that 12, 13-diHOME—a representative oxidation product of LA—was detected at low levels in the LA-only condition but was undetectable when BHT was co-administered (Table 4), confirming that BHT effectively suppressed its formation. However, the absolute amount of 12, 13-diHOME detected was minimal, and other oxidized lipid species were present in both conditions at comparable levels (Table 4). This indicates that while BHT partially altered the oxidation profile of LA, the overall degree of oxidation was limited under experimental conditions.

Furthermore, co-treatment with BHT did not affect the antiviral effect of LA (Figure 7A), and no cytotoxicity was observed in HRV16-infected cells treated with both LA and BHT (Figure 7B). These findings indicate that LA undergoes minimal oxidation under these experimental conditions, and more importantly, that its antiviral activity is primarily attributable to LA itself, rather than to its oxidative metabolites. Therefore, LA is sufficient to exert antiviral efficacy without the need for antioxidant supplementation.

Table 4. Concentration of LA and oxylipins in cell media (n = 1)

Sample	LA	12(13)-DiHOME	9(10)-DiHOME	13(S)-HODE	12(13)-EpOME	9(S)-HODE	9(10)-EpOME	13-OxoODE	9-OxoODE
RPMI only	0	0	0	0	0	0	0	0	0
RPMI + LA	18046	0.36	0.34	30.62	28.86	23.15	27.31	8.88	9.56
RPMI + BHT + LA	12514.2	0	0.24	22.78	22.79	20.75	19.97	9.18	12.96

Unit of concentration: ng/ml; BHT: butylated hydroxytoluene; LA: linoleic acid; DiHOME: dihydroxyoctadecenoic acid; HODE: hydroxy-octadecadienoic acids; EpOME: epoxyoctadecenoic acids (EpOMEs); OxoODE: oxo-octadecadienoic acid

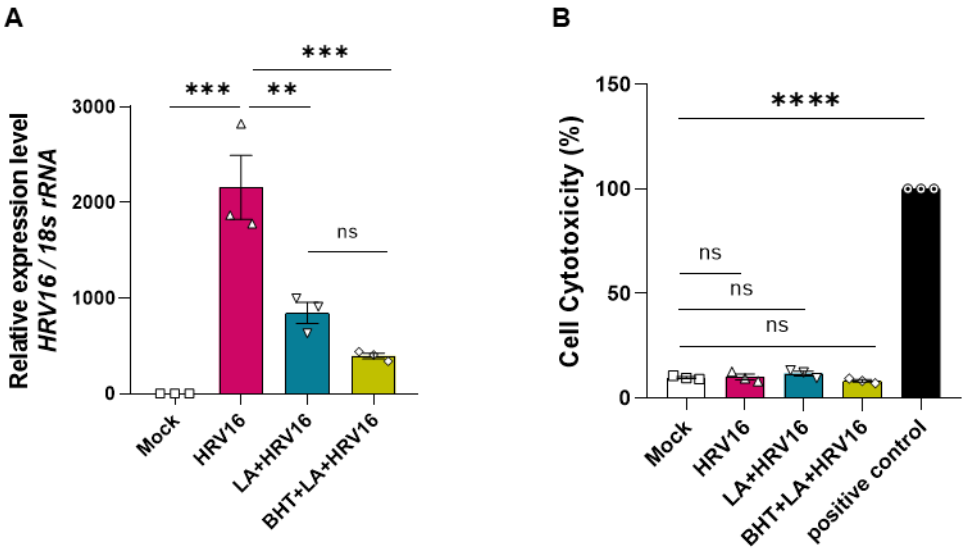

Figure 7. LA treatment has antiviral effect regardless of presence of butylated hydroxytoluene (BHT) in BEAS-2B Cells. (A) Relative HRV16 mRNA expression levels in LA (50 μM) treated with or without BHT (25 μM) in BEAS-2B cells were measured by qPCR at 24 hpi (n = 3). (B) Cell cytotoxicity in HRV16, HRV16 with LA, or HRV16 with BHT contained LA BEAS-2B cell media was measured by an LDH assay at 24 hpi (n = 3). Results are shown as the mean ± SEM; *p < 0.05; **p < 0.01; ***p < 0.001; ****p < 0.0001 using one-way ANOVA with Tukey's multiple comparisons test.

3.4. GPR40/GPR120 dual agonist GW9508 shows antiviral effect in HRV16 infected BEAS-2B cells

GPR40 (FFAR1) and GPR120 (FFAR4) are widely recognized as receptors for long-chain fatty acids[18]. Therefore, GW9508, a dual agonist for GPR40/GPR120, was used for the activation of receptors to investigate whether GPR40/120 is involved in the antiviral effect of LA (Figure 8A). Treatment with GW9508 decreased HRV16 mRNA expression levels at 24 hpi, and this effect was comparable to that of treatment with LA (Figure 8B). Furthermore, treatment with GW9508 also reduced HRV16 capsid proteins in the cell lysate and viral load in the media, lowering both to levels similar to those observed in the LA-treated group (Figure 8C, D). These results suggest that the antiviral effect of LA may be mediated through GPR40/GPR120.

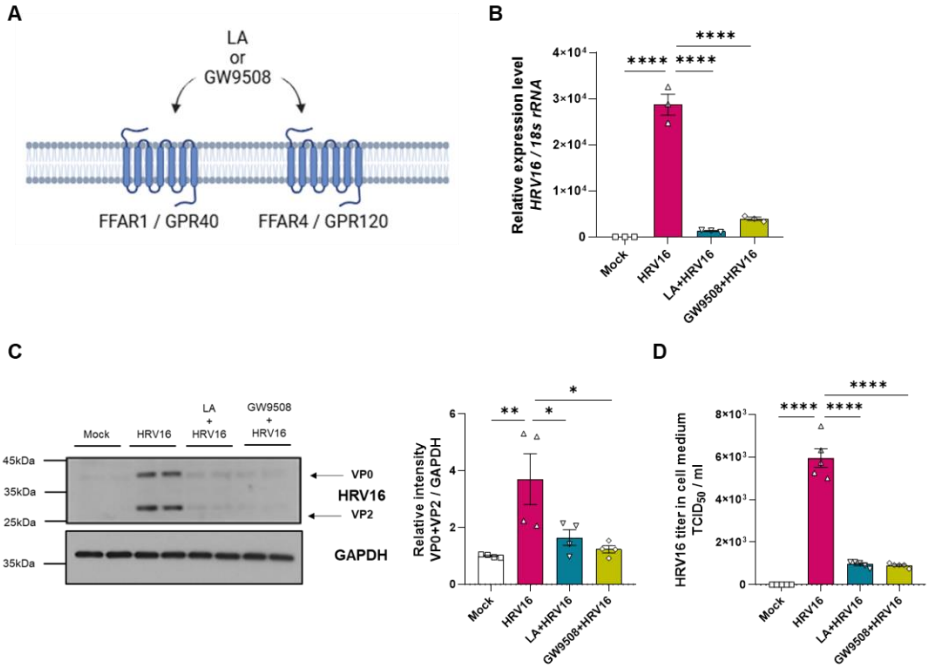

Figure 8. GPR40/GPR120 dual agonist GW9508 shows antiviral effect in HRV16 infected BEAS-2B cells. (A) Schematic illustration of working model between GPR40/GPR120 and GW9508 and LA in airway epithelial cells. (B) Relative HRV16 mRNA expression levels in Mock, HRV16, LA (50 μM) + HRV16, and GW9508 (50 μM) + HRV16 treated BEAS-2B cells were measured by qPCR at 24 hpi (n = 3). (C) Representative immunoblot analysis of HRV16 capsid proteins (VP0, VP2) in BEAS-2B cell lysates from each group at 24 hpi (n = 4). Relative intensity of viral protein levels was quantified with image J. The intensity of VP0, VP2 proteins was normalized with GAPDH. (D) Viral load in each group of BEAS-2B cells was measured by $TCID_{50}$ in the culture supernatant at 24 hpi (n = 5). Results are shown as the mean ± SEM; *p < 0.05; **p < 0.01; ***p < 0.001; ****p < 0.0001 using one-way ANOVA with Tukey's multiple comparisons test.

3.5. LA treatment induces transcriptional alteration in HRV infected BEAS-2B cells

To identify transcriptional changes in BEAS-2B cells in response to LA treatment, bulk mRNA sequencing was performed on Mock, HRV16-infected (V), LA-treated (L), and HRV16-infected with LA (LV) samples at 4 hpi. Interestingly, there was little difference between Mock and V, indicating that viral infection did not induce alterations in gene expression in BEAS-2B cells (Figure 9A). In contrast, LA treatment induced significant alterations in gene expression compared to mock or HRV16 infection (Figure 9A). Therefore, I compared altered genes by comparing between V group and LV group. To investigate the gene set GOBP: Defense Response to Virus (GO: 0051607), comprising 312 genes associated with antiviral responses that protect cells (Figure 8B).

Through RT-qPCR, the top five genes identified in the gene set were validated, including Deleted in Malignant Brain Tumors 1 (DMBT1), ISG20, Tripartite Motif Containing 35 (TRIM35), Interferon Regulatory Factor 1 (IRF1), and Tripartite Motif Containing 27 (TRIM27). Among these, DMBT1, ISG20, and TRIM27 were upregulated in the LV group compared to the V group, while TRIM35 and IRF1 showed no significant differences (Figure 9C). DMBT1 is known to influence viral entry by binding directly to envelope proteins [52-54]; however, as HRV is a non-enveloped virus, it is unlikely to exhibit antiviral activity against HRV. Consequently, DMBT1 was excluded from further experiments. Although TRIM27 was significantly upregulated in the LV group, its fold change was modest (below 1.5-fold; Figure 9C). In contrast, ISG20 exhibited a pronounced upregulation in the LV group and showed the second-highest signal-to-noise ratio (Figure 9B), with a fold change exceeding 3.0 (Figure 9C). Additionally, ISG20 is well-documented for its antiviral role, particularly through RNase activity in airway epithelial cells [26,55]. Based on these findings, ISG20 was selected as the target gene mediating the antiviral effects of LA in BEAS-2B cells.

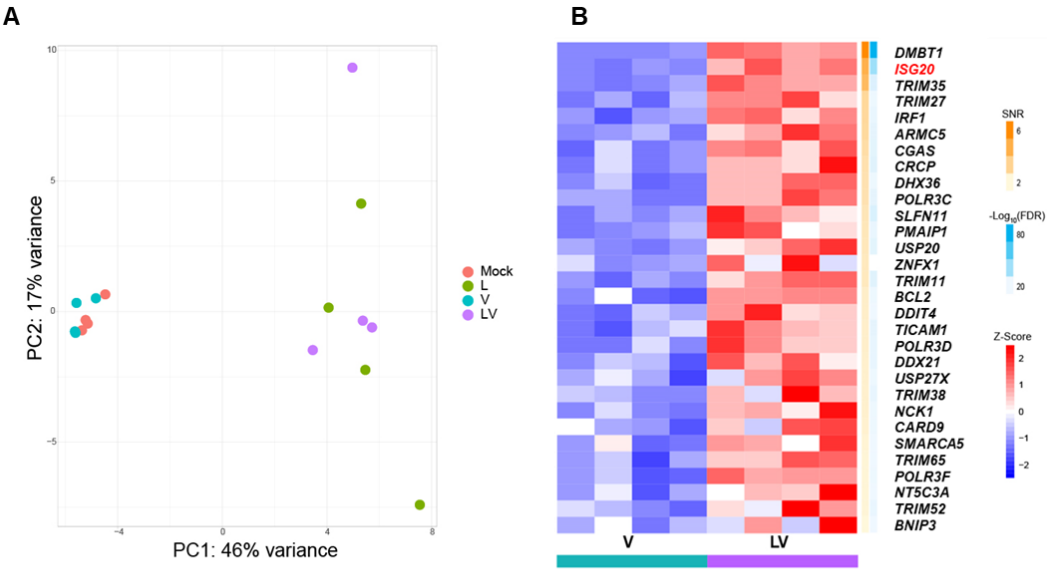

C

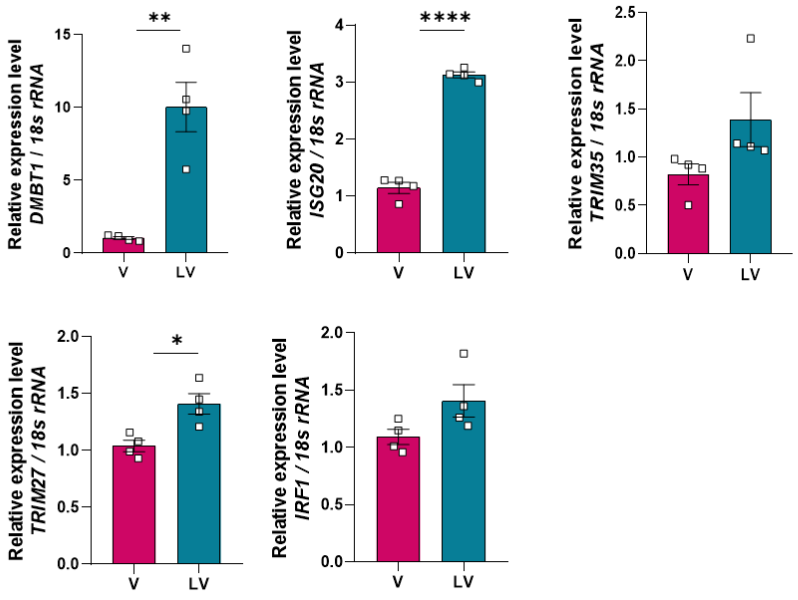

Figure 9. LA treatment induces transcriptional alteration in HRV infected BEAS-2B cells. (A) Principal coordinates analysis (PCA) plot among Mock, HRV16-infected (V), LA-treated (L), HRV16-infected with LA (LV) groups (n = 4). (B) The heat map displays the normalized expression levels of genes between the V and LV groups within the "Defense Response to Virus" (GO: 0051607) gene set. The top 30 genes with the highest signal-to-noise ratio (SNR) values are shown in decreasing order (n = 4). (C) Relative mRNA expression levels in each group were measured by qPCR at 4 hpi (n = 4). Results are shown as the mean ± SEM; *p < 0.05; **p < 0.01; ***p < 0.001; ****p < 0.0001 using Student's t-test.

3.6. Upregulation of ISG20 by LA is dependent on the NF-κB pathway in BEAS-2B cells

Several previous studies have shown that HRV infection does not induce an increase in type I interferon (IFN-I) production in airway epithelial cells [56-58]. In line with previous studies, HRV16 infection did not increase IFN-I secretion in BEAS-2B cells (Figure 10A). Furthermore, ISG20 mRNA level was not increased in HRV16 infected group at 4 hpi (Figure 10B). This could be the upregulation of ISG20 in induced by LA treatment not by HRV infection. Thus, in my BEAS-2B cell system, contributions to IFN-I are likely minimal, based on the study of the regulatory mechanism underlying ISG20 upregulation following LA treatment.

In a previous study, activation of NF-κB is known to directly induce ISG20 expression in endothelial cells [30]. I observed that NF-κB p65 phosphorylation was higher in LA-treated cells compared to HRV16-infected cells at 30 minutes post-infection (Figure 11A). To determine whether NF-κB inhibition affects ISG20 expression, caffeic acid phenethyl ester (CAPE) was used as an NF-κB inhibitor. The treatment CAPE reduced phosphorylation of p65 (Figure 11B). Upon inhibition of NF-κB using CAPE, ISG20 expression was decreased at 24 hpi (Figure 11C). These results indicate that the upregulation of ISG20 expression in response to LA treatment is dependent on NF-κB activation in BEAS-2B cells.

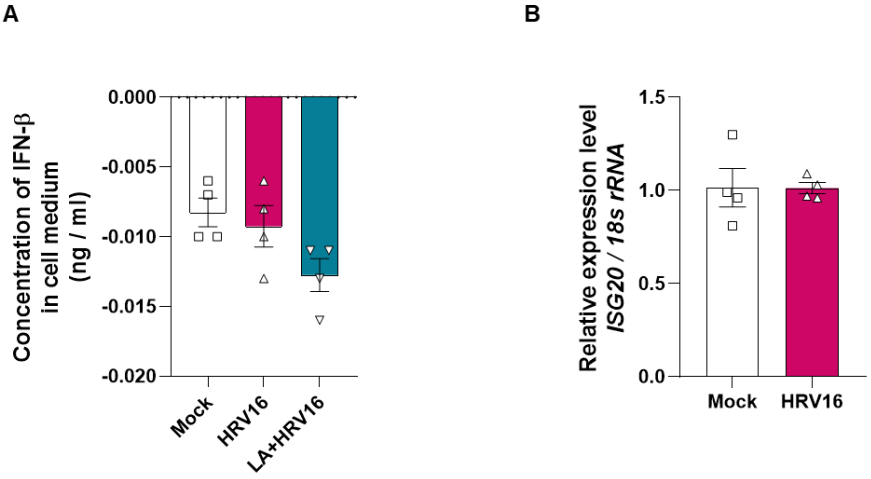

Figure 10. HRV16 infection does not induce IFN-β or ISG20 upregulation in BEAS-2B cells. (A) Secretion of IFN-β by HRV16 infection was measured by enzyme-linked immunosorbent assay (ELISA) in cell supernatant at 24 hpi (n = 4). (B) ISG20 mRNA expression levels were quantified by qPCR at 4 hpi in BEAS-2B cells (n = 4). Results are shown as the mean ± SEM; *p < 0.05; **p < 0.01; ***p < 0.001; ****p < 0.0001 using one-way ANOVA with Tukey's multiple comparisons test or Student's t-test.

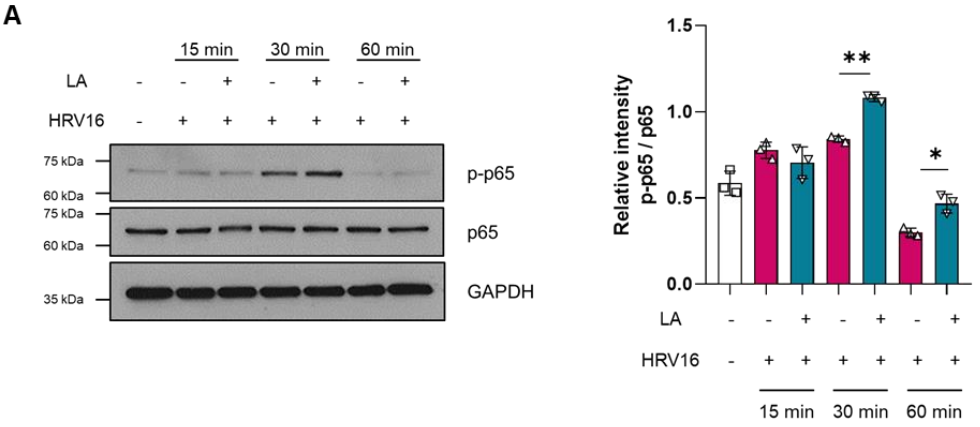

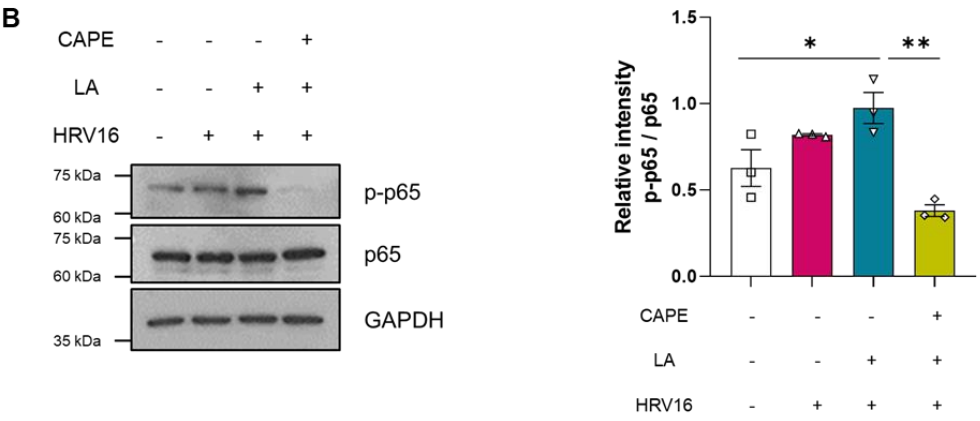

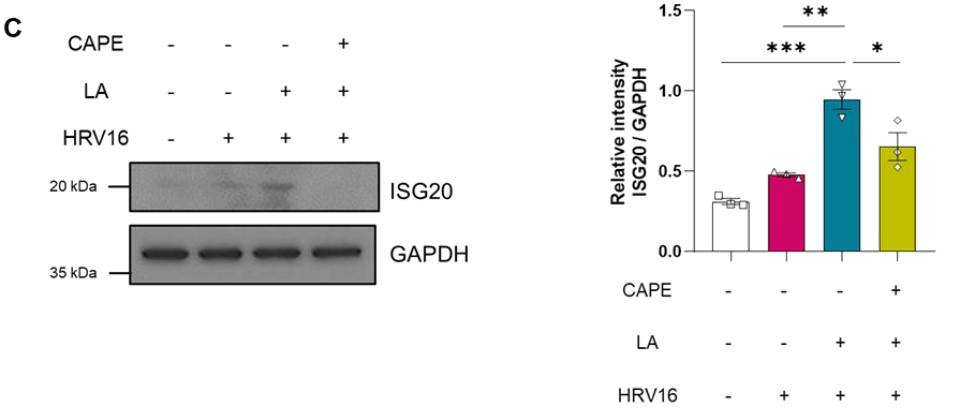

Figure 11. Upregulation of ISG20 by LA is dependent on the NF-κB pathway in BEAS-2B cells. (A) Representative immunoblot analysis showing time-dependent phosphorylation of p65 (p-p65) proteins following LA (50 μM) treatment in BEAS-2B cells (n = 3). (B) Representative immunoblot analysis of p-p65 protein levels following treatment with the NF-κB inhibitor CAPE (20 μM) for 30 min, prior to LA (50 μM) treatment in BEAS-2B cells. Samples were collected at 30 min post-infection. (n = 3). (C) Representative immunoblot analysis of ISG20 protein levels at 24 hpi in BEAS-2B cells (n = 3). Relative intensity of each protein level was quantified with Image J. The intensity of the proteins was normalized to GAPDH or p65. Results are shown as the mean ± SEM; *$p < 0.05$; **$p < 0.01$; ***$p < 0.001$; ****$p < 0.0001$ using one-way ANOVA with Tukey's multiple comparisons test.

3.7. ISG20 is responsible for antiviral effect of LA in BEAS-2B cells

Next, to investigate whether the antiviral effect of LA treatment directly mediated by ISG20, lentivirus-based knockdown system was used in BEAS-2B cells. It was confirmed that the transcriptional level of ISG20 was reduced in the ISG20-specific short hairpin RNA (sh-ISG20) lentivirus-treated group compared to the scramble short hairpin RNA (sc-shRNA) lentivirus-treated group (Figure 12A). Additionally, protein expression was decreased in the sh-ISG20 lentivirus-treated group compared to sc-shRNA group (Figure 12B). The HRV16 titer in the cell culture media was significantly higher in the sh-ISG20 group compared to the sc-shRNA group, both in the absence and presence of LA (Figure 12C). These findings collectively suggest that the antiviral effect of LA against HRV16 is ISG20-dependent.

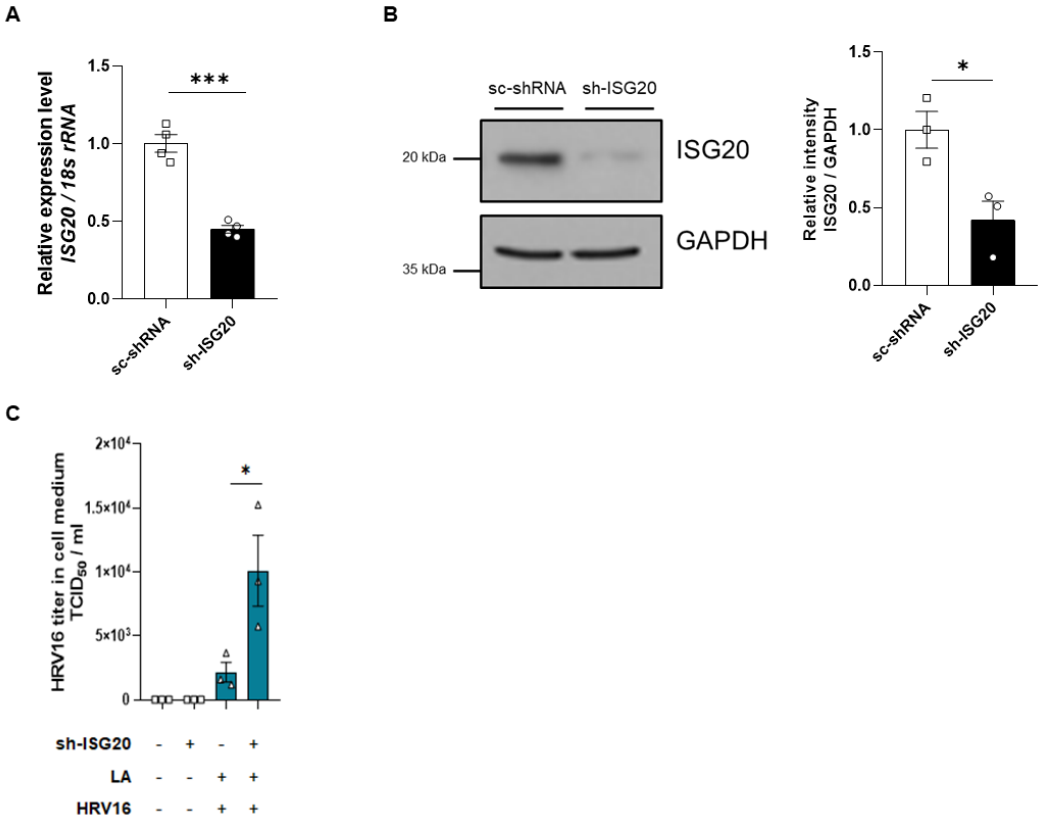

Figure 12. ISG20 is responsible for antiviral effect of LA in BEAS-2B cells. (A) Relative expression level of ISG20 mRNA between scrambled short hairpin RNA (sc-shRNA) or ISG20 specific short hairpin RNA (sh-ISG20) treated group (n = 4). (B) Representative immunoblot analysis of ISG20 proteins in sc-shRNA treated BEAS-2B cells and shISG20 treated BEAS-2B cells (n = 3). Relative intensity of protein levels was quantified with image J. The intensity of the proteins was normalized to GAPDH. (C) Viral load in HRV16 infected BEAS-2B cells was measured by $TCID_{50}$ in culture supernatant (n = 3). Results are shown as the mean ± SEM; *p < 0.05; **p < 0.01; ***p < 0.001; ****p < 0.0001 using Student's t-test.

3.8. Respiratory administration of Na-LA enhances antiviral effects in an HRV-infected mouse model

To investigate the antiviral effects of LA in an in vivo HRV infection model, I first evaluated different LA formulations for respiratory delivery. Notably, BSA-conjugated LA (BSA-LA), which is commonly used in in vitro settings, induced elevated levels of the proinflammatory cytokine IL-6 in bronchoalveolar lavage (BAL) fluid, suggesting that this formulation may exacerbate airway inflammation (Figure 13A). This observation is consistent with previous reports that BSA can elicit immune responses when delivered systemically or locally [59]. In contrast, sodium linoleate (Na-LA), a water-soluble form of LA, did not trigger such inflammatory responses (Figure 13A). Furthermore, BSA-LA failed to confer antiviral protection in the HRV1B-infected mouse model and did not reduce IL-6 levels (Figure 13B, 13C), whereas Na-LA treatment exhibited both anti-inflammatory and antiviral effects. Collectively, these findings indicate that BSA-conjugation is not a suitable approach for in vivo evaluation of antiviral properties of LA, and that Na-LA is a more viable and physiologically relevant formulation for intranasal delivery.

Next, Balb/c mice were intranasally inoculated with HRV1B, with or without Na-LA treatment (Figure 14A). HRV1B titers in BAL fluid peaked at 8 hpi, while no viral titers were detected following inoculation with UV-inactivated HRV1B (Figure 14B). Notably, Na-LA treatment significantly reduced viral loads in BAL fluid at 8 hpi compared to the untreated HRV1B-infected group (Figure 14B). Additionally, the antiviral effect of Na-LA was dose-dependent (Figure 14C, D), consistent with previous in vitro findings.

Targeted metabolomics analysis revealed that Na-LA treatment increased LA levels in BAL fluid, with no significant changes observed in its oxidative metabolites, including HODEs, Oxo-ODEs, EpOMEs, and DiHOMEs, compared to the mock group (Figure 15). These results, consistent with in vitro data (Table 4 and Figure 7), suggest that the antiviral effect of Na-LA is mediated by LA itself, independent of its conversion to oxylipins. To further examine the specificity of this effect, comparative analysis of various LCFAs including oleic acid (OA), palmitic acid (PA), and palmitoleic acid (PO), revealed that only LA exhibited a significant antiviral effect against HRV, indicating that this activity is specific to LA among tested LCFAs (Figure 16).

Furthermore, the LA concentration detected in BAL fluid (~1,000 to 4,000 ng/ml; Figure 14A) corresponds to approximately 3.6–14.5 μM, which is within the micromolar range. Although this is lower than typical plasma levels reported to be approximately 800 μM [60] it is important to note that BAL fluid represents the local mucosal compartment, where even micromolar levels can be functionally significant. Taken together, these results demonstrate that intranasally delivered LA reaches effective local concentrations in the respiratory tract, supporting its utility as a potential therapeutic strategy against HRV infection.

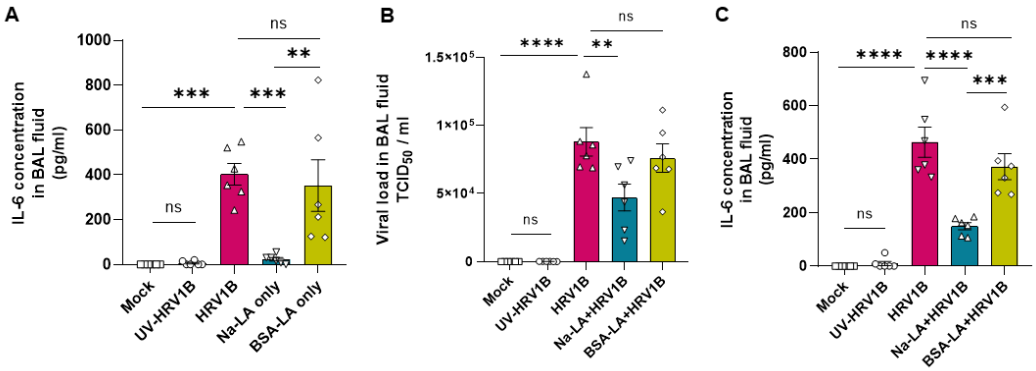

Figure 13. Pro-inflammatory cytokine IL-6 levels and viral loads in mouse BAL fluids following Na-LA or BSA-LA treatment. (A) IL-6 levels in BAL fluids were measured by ELISA in mice treated with Na-LA only or BSA-LA only (n = 6). (B) Viral loads in BAL fluids were quantified in mice from the following groups: mock, UV-inactivated HRV1B, HRV1B alone, Na-LA + HRV1B, and BSA-LA + HRV1B (n = 6). (C) IL-6 levels in mouse BAL fluids were measured by ELISA in the same experimental groups as in (B). Results are shown as the mean ± SEM; *p < 0.05; **p < 0.01; ***p < 0.001; ****p < 0.0001 using one-way ANOVA with Tukey's multiple comparisons test.

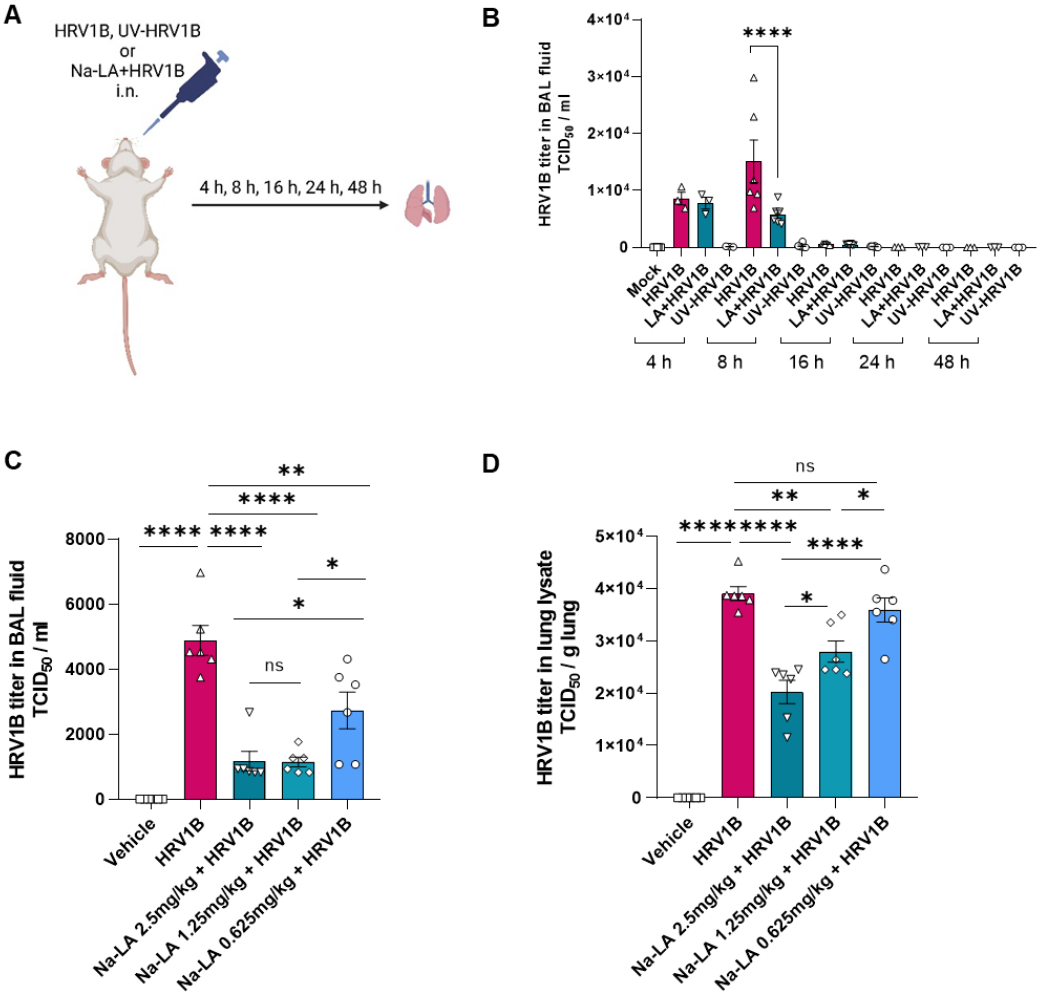

Figure 14. Dose-dependent antiviral effects of respiratory administration of sodium linoleate (Na-LA) in an HRV-infected mouse model. (A) Schematic image of in vivo HRV1B infection experiment. (B) Viral load of HRV1B in mouse BAL fluid was measured by $TCID_{50}$ in time-dependent manner (n = 3 for 4, 24, 48 h, n = 6 for 8 h, 16 h). (C) Viral load of HRV1B in BAL fluid was measured by $TCID_{50}$ in 8 hpi. (n = 6). (D) Viral load of HRV1B in mouse lung was measured by $TCID_{50}$ in 8 hpi (n = 6). Data shown are representative of two independent experiments. Results are shown as the mean ± SEM; *p < 0.05; **p < 0.01; ***p < 0.001; ****p < 0.0001 using one-way ANOVA with Tukey's multiple comparisons test.

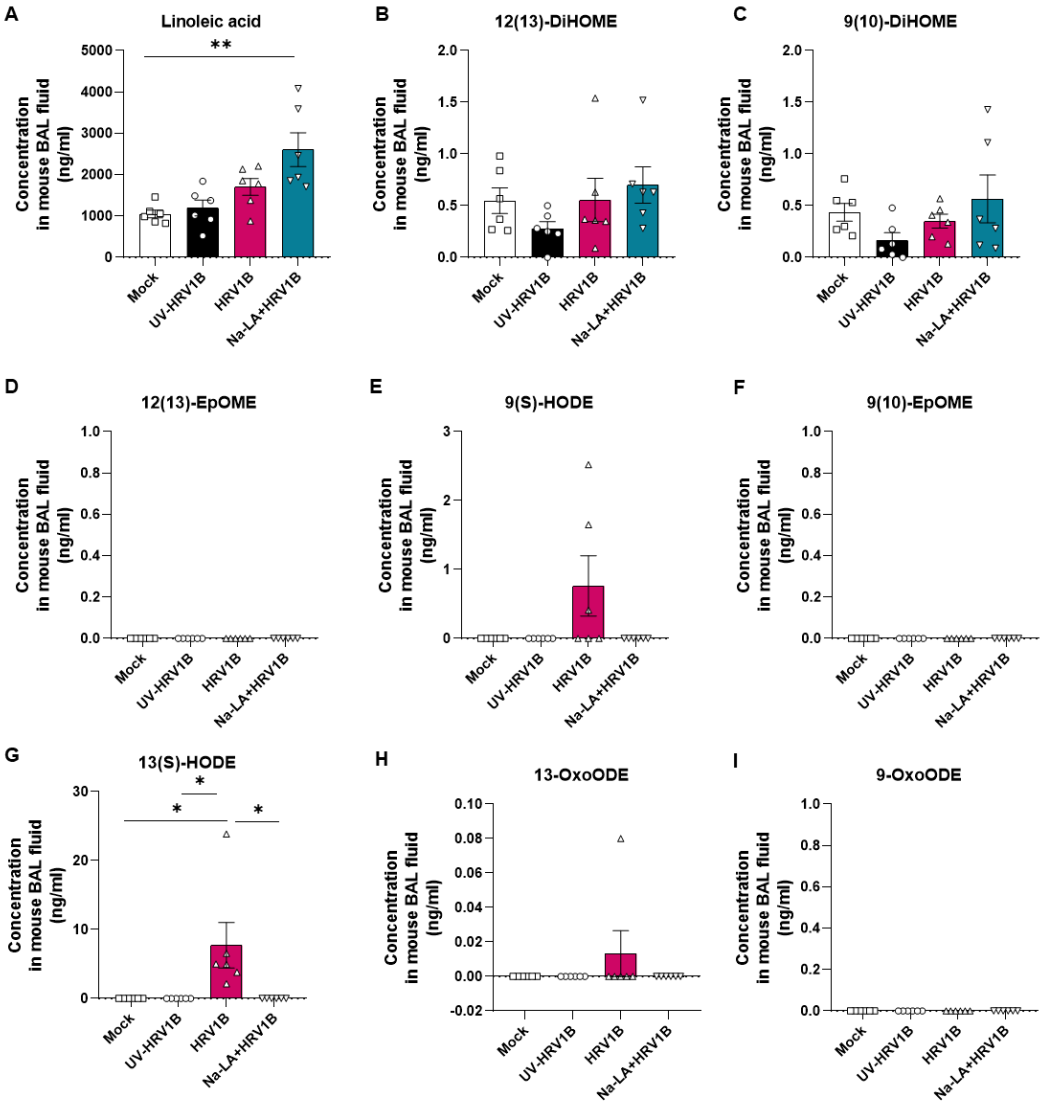

Figure 15. Quantification of LA and oxylipins in mouse BAL fluid. (A) Quantification of metabolite concentrations in mouse BAL fluids. Concentration of LA and oxylipins in mouse BAL fluid was analyzed by LC-MS/MS-based targeted metabolomics analysis (n = 6). Data shown are representative of two independent experiments. Results are shown as the mean ± SEM; *p < 0.05; **p < 0.01; ***p < 0.001; ****p < 0.0001 using one-way ANOVA with Tukey's multiple comparisons test.

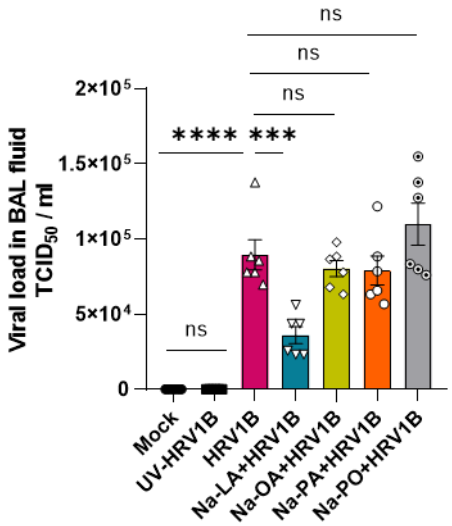

Figure 16. Only Na-LA treatment has antiviral effect among various LCFAs in BAL fluids. Viral load of HRV1B in BAL fluid was measured by $TCID_{50}$ in 8 hpi. (n = 6). Results are shown as the mean ± SEM; *p < 0.05; **p < 0.01; ***p < 0.001; ****p < 0.0001 using one-way ANOVA with Tukey's multiple comparisons test.

3.9. Respiratory administration of Na-LA exerts GPR40/120-mediated antiviral effects in an HRV-infected mouse

In prior experiments conducted in BEAS-2B cells, it was demonstrated that the antiviral effect of LA is mediated through GPR40/GPR120 signaling (Figure 8). To determine whether this mechanism is relevant in the HRV-infected mouse model, HRV1B titers and lung histopathology were measured in mice pretreated with GPR40 and GPR120 antagonists (intraperitoneally injected AH7614 to inhibit GPR120 and GW1100 to inhibit GPR40) (Figure 17A). Interestingly, treatment with these antagonists reversed the reduction in HRV1B titers observed with Na-LA treatment, restoring viral loads in BAL fluid (Figure 17B) and lung lysates (Figure 17C). Additionally, antagonists reversed the effects on cell infiltration in BAL fluid (Figure 17D), protein levels in BAL fluid (Figure 17E), cytokine production (Figure 17F, G), and lung pathology (Figure 17H, I). Furthermore, the Na-LA-induced increase in ISG20 expression was attenuated by GPR40/120 antagonists (Figure 18A-B).

To assess whether ISG20 upregulation by Na-LA treatment is dependent on interferon signaling, levels of IFN-β and IFN-λ2/3 were measured in BAL fluids. Notably, Na-LA treatment did not increase the expression of IFN-β or IFN-λ2/3 (Figure 19). These findings suggest that ISG20 upregulation induced by LA occurs independently of interferon signaling.

Collectively, these results demonstrate that respiratory administration of LA enhances antiviral effects against HRV through a GPR40/120-dependent mechanism (Figure 20). Furthermore, my data suggest that the antiviral activity of LA is mediated via a GPR40/120-ISG20 signaling axis, rather than through interferon signaling pathways.

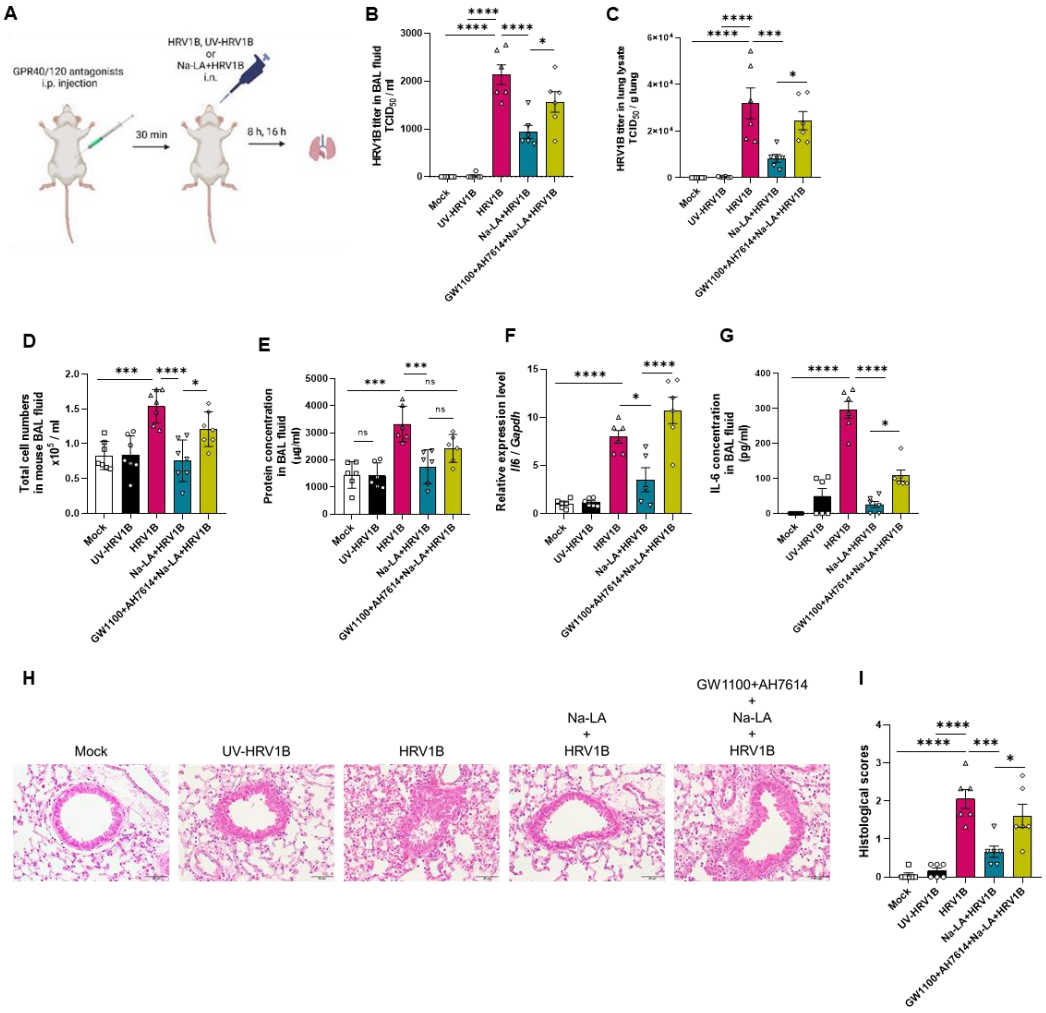

Figure 17. Respiratory administration of Na-LA enhances antiviral effects via a GPR40/120-dependent mechanism in an HRV-infected mouse model. (A) Schematic image of the in vivo GPR40/120 antagonists treatment experiment. (B) Viral load of HRV1B in BAL fluid was measured by $TCID_{50}$ in 8 hpi (n = 6). (C) Viral load of HRV1B in mouse lung was measured by $TCID_{50}$ in 8 hpi (n = 6). (D) Total cell number in BAL fluid was measured. (n = 6). (E) Protein concentrations in BAL fluid were measured using the BCA assay in 8 hpi (n = 6). (F) Relative *Il6* mRNA expression levels in lung lysates were measured by qPCR at 8 hpi normalized with *Gapdh* (n = 6). (G) IL-6 was measured by ELISA in mouse BAL fluids at 8 hpi (n = 6). (H) Representative hematoxylin and eosin (H&E) staining of lung sections (40X) at 16 hpi (n = 6). (I) Histology scores were presented as a bar graph (n = 6). (Results are shown as the mean ± SEM; *p < 0.05; **p < 0.01; ***p < 0.001; ****p < 0.0001 using one-way ANOVA with Tukey's multiple comparisons test.

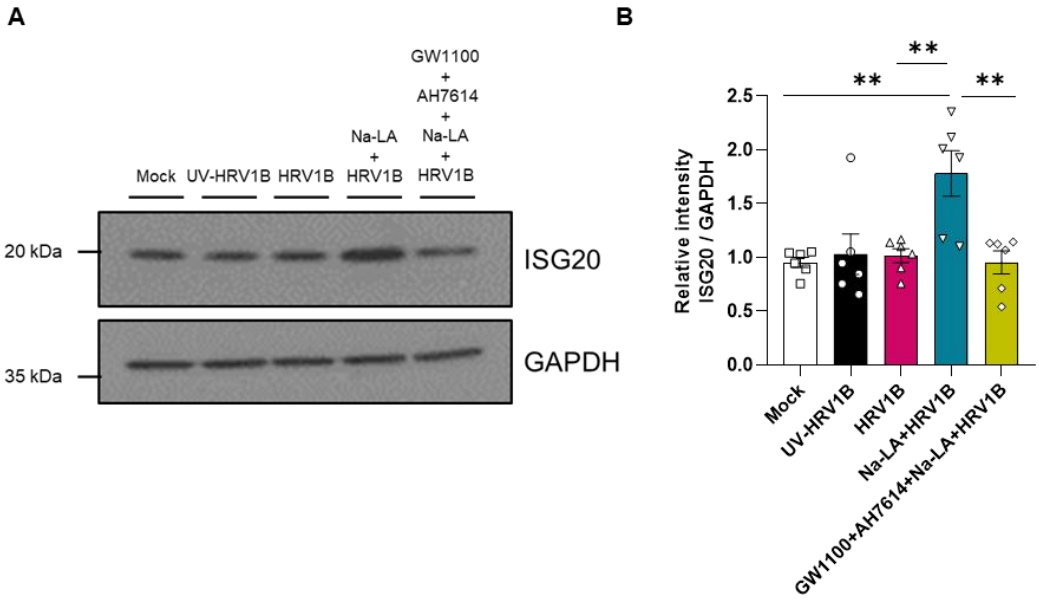

Figure 18. The regulation of ISG20 by Na-LA treatment is GPR40/120-dependent in an HRV-infected mouse model. (A) Representative immunoblot analysis of ISG20 proteins in each group at 8 hpi (n = 6). (B) Relative intensity of protein levels was quantified with image J. The intensity of ISG20 proteins was normalized with GAPDH. Data shown are representative of two independent experiments, each with technical duplicates. Results are shown as the mean ± SEM; *p < 0.05; **p < 0.01; ***p < 0.001; ****p < 0.0001 using one-way ANOVA with Tukey's multiple comparisons test.

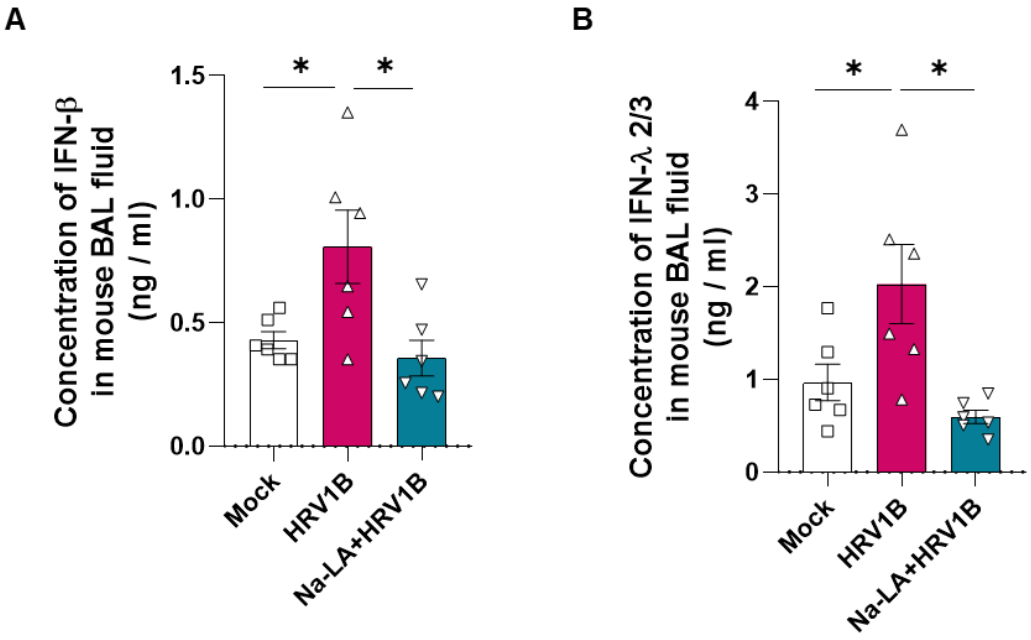

Figure 19. No enhancement in the expression of interferons by Na-LA treatment. (A) IFN-β was measured by ELISA in mouse BAL fluids (*n* = 3 for Mock, *n* = 8 for HRV1B, Na-LA+HRV1B). (B) IFN-λ 2/3 was measured by ELISA in mouse BAL fluids (*n* = 3 for mock, *n* = 8 for HRV1B, Na-LA+HRV1B). Results are shown as the mean ± SEM; **p* < 0.05; ***p* < 0.01; ****p* < 0.001; *****p* < 0.0001 using one-way ANOVA with Tukey's multiple comparisons test.

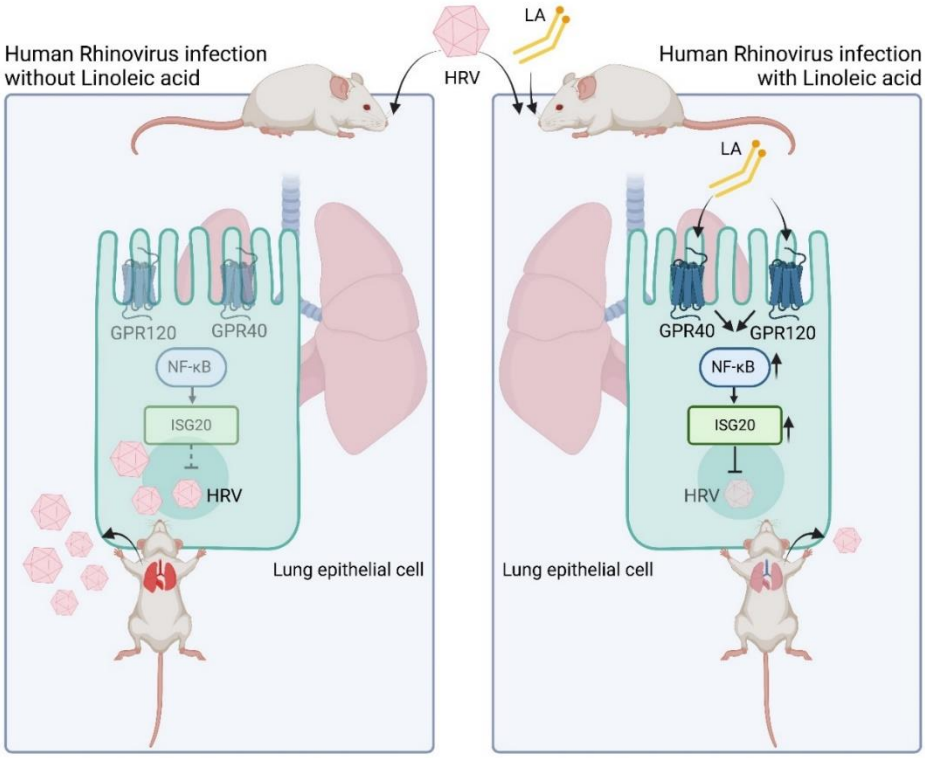

Figure 20. Schematic diagram of the antiviral effect of the LA in HRV infection. Respiratory administration of LA enhances antiviral effects against HRV through the upregulation of ISG20 via a GPR40/120-dependent mechanism.

4. Discussion

In this study, I elucidated that LA plays an antiviral role in HRV infection. These results revealed that treatment with LA induced antiviral effects by increasing ISG20 expression via the NF-κB pathway in airway epithelial cells. LA cannot be produced by the host itself but must be obtained through food intake [61]. However, LA was detected in human nasal fluid using targeted LC/MS analysis (Figure 2). One potential explanation for this finding is that LA may be derived from the upper airway microbiome. According to previous studies, commensal bacteria such as *Corynebacterium*, *Staphylococcus*, and *Dolosigranulum* are known to play an important role in protecting against severe respiratory symptoms [62-64]. Among these strains, *Corynebacterium accolens* (*C. accolens*) has been associated with the enrichment of free fatty acids, including LA, and has been shown to participate in anti-pneumococcal activity [65]. Recently, strains of *C. accolens* have been shown to play a protective role in SARS-CoV-2 infection [66]. When additional Na-LA is administered during rhinovirus infection, a protective effect is observed in this study, confirming that LA plays an important role during rhinovirus infection.

Among the G protein-coupled receptors, GPR40 and GPR120 are receptors for long-chain fatty acid ligands. According to previous studies, GPR40/120 are well known as receptors for omega-3 fatty acids and are expressed in lung and colon epithelial cells [67]. GPR40 has been reported to participate in tight junction assembly in an AMP-activated protein kinase (AMPK)-dependent manner in human airway epithelial cells [68]. Although GPR120 is also mainly expressed in airway epithelial cells, its role has not been extensively studied yet [69,70]. Recently, *Clostridium butyricum*-induced ω-3 fatty acid, 18-HEPE, was found to promote IFN-lambda production through GPR120 and IRF1/7 activation [22]. Similar to the attenuation of influenza virus, this study suggested that local treatment with LA induces an antiviral effect through GPR40/120 in airway epithelial cells. Additionally, GPR120 activation has been reported to suppress IL-4 and IL-13-induced allergic inflammation and block airway epithelium remodeling by inhibiting STAT6 and Akt phosphorylation [71]. Since allergic inflammatory diseases induced by rhinovirus infection are related to IL-4 and IL-13 [72-74], treatment with LA may alleviate these diseases through GPR120 activation.

In my results, an antiviral effect of LA was observed when it was administered prior to, simultaneously with, or following rhinovirus infection in airway epithelial cells (Figure 6). Notably, the antiviral efficacy was shown to be independent of the timing of administration, indicating that the effect is not limited to viral entry or early infection stages. This observation suggests that the antiviral activity of LA is mediated through intracellular mechanisms rather than extracellular inhibition of viral binding or entry.

Therefore, bulk mRNA sequencing was performed in BEAS-2B cells to investigate transcriptomic changes induced by LA treatment. At 4 hpi, several genes including ISG20 were found to be upregulated in response to LA (Figure 9). Among these, the expression of DMBT1 (also known as gp340) was notably increased, as confirmed by mRNA sequencing analysis (Figure 9B, C). DMBT1 has previously been shown to protect airway epithelial cells by binding to the hemagglutinin of the influenza virus, as well as to a broad range of bacteria, including *Streptococcus* species [52,75,76]. Based on these findings, it is suggested that LA treatment may enhance airway protection not only by exerting antiviral effects, but also by promoting antibacterial defense mechanisms via DMBT1 upregulation.

ISG20 is known to directly degrade viral RNA, and several mechanisms have been reported [26]. The three mechanisms of viral inhibition by ISG20 are direct viral RNA degradation [28,29,77,78], direct degradation of deaminated viral DNA [79,80], and IFN induction along with IFIT1-mediated translation inhibition of viral RNA [81,82]. According to previous research, it was unable to detect measurable type I IFN protein secretion from HRV-infected epithelial cells [56-58]. Similar to those of previous studies, showing that IFN was not induced during rhinovirus infection in BEAS-2B cells (Figure 10). Unlike the in vitro data, IFN was induced upon HRV infection in vivo (Figure 19). However, its expression levels were decreased by treatment with LA (Figure 19). These findings suggest that early viral inhibition was induced through the direct induction of NF-κB-ISG20 by LA treatment, rather than through the IFN-dependent ISG20 induction.

In this study, I found that ISG20 expression was induced by treatment with LA, leading to activation of NF-κB pathway in airway epithelial cells (Figure 11). This phenomenon is similar to the induction of IFN-like gene *Vago5* expression through the ERK-NF-κB pathway by treatment with LA during WSSV infection [83], and the NF-κB pathway was involved in ISG20 expression [30]. Taken together, these results suggest that LA induces ISG20 expression through NF-κB activation, independently of IFN-I signaling.

This study has several limitations. Although it was confirmed that ISG20 involvement in vitro via knockdown studies (Figure 12), further work using ISG20 knockout mice would be necessary to fully establish its role in vivo. Additionally, the downstream signaling cascade from GPR40/120 to ISG20 via NF-κB remains unclear.

Despite these limitations, this study provides the first evidence that locally administered LA exhibits antiviral activity against HRV both in vivo and in vitro. A novel signaling axis involving GPR40/120 and ISG20 was identified, revealing a previously unrecognized mechanism by which host lipid signaling modulates viral replication and inflammatory responses.

Furthermore, it was demonstrated that intranasally administered LA is effectively delivered to the airway without oxidation (Figure 15). Airway-delivered LA was shown to significantly reduce both viral burden and airway inflammation. Notably, among the various long-chain fatty acids (LCFAs) tested, only LA demonstrated such antiviral and anti-inflammatory effects in vivo, indicating that these therapeutic benefits are specific to LA (Figure 16). This noninvasive mode of delivery enables localized therapeutic action while minimizing systemic exposure to LA, thereby potentially avoiding adverse effects associated with elevated circulating LA levels following oral administration [84].

Given the central role of HRV in exacerbating respiratory conditions such as asthma, COPD, allergic rhinitis, and the common cold, our findings suggest that intranasal Na-LA may serve as a promising prophylactic or therapeutic strategy against HRV-associated airway diseases. Moreover, since LA has also been reported to inhibit SARS-CoV-2 by binding to the viral spike protein and altering its conformation [15,16], it is conceivable that LA-based interventions could be effective against a broader spectrum of respiratory viruses beyond HRV.

5. CONCLUSION

This study highlights the protective role of linoleic acid (LA) against Human Rhinovirus (HRV) infection, a major contributor to respiratory diseases. I demonstrated that LA treatment reduces HRV16 infectivity in human airway epithelial cells by inducing the expression of the antiviral protein ISG20, which effectively inhibits HRV replication. Furthermore, the antiviral effects of LA were shown to be mediated through G-protein coupled receptors (GPR) 40 and 120, as well as the activation of the NF-κB signaling pathway. In vivo, intranasal administration of sodium linoleate (Na-LA) attenuated HRV-induced pathophysiology in mice in a GPR40/120-dependent manner, further supporting the potential therapeutic benefits of Na-LA. Collectively, these findings provide compelling evidence that LA may serve as a promising therapeutic candidate for the treatment of HRV infections and related respiratory diseases, offering a novel strategy to alleviate the burden of viral respiratory illnesses.

REFERENCES

1. Winther B. Rhinoviruses. International Encyclopedia of Public Health 2008:577.
2. Pitkäranta A, Starck M, Savolainen S, Pöyry T, Suomalainen I, Hyypiä T, et al. Rhinovirus RNA in the maxillary sinus epithelium of adult patients with acute sinusitis. Clinical infectious diseases 2001;33:909-11.
3. Winther B, Alper CM, Mandel EM, Doyle WJ, Hendley JO. Temporal relationships between colds, upper respiratory viruses detected by polymerase chain reaction, and otitis media in young children followed through a typical cold season. Pediatrics 2007;119:1069-75.
4. Curren B, Ahmed T, Howard DR, Ullah MA, Sebina I, Rashid RB, et al. IL-33-induced neutrophilic inflammation and NETosis underlie rhinovirus-triggered exacerbations of asthma. Mucosal Immunology 2023;16:671-84.
5. Papadopoulos NG, Christodoulou I, Rohde G, Agache I, Almqvist C, Bruno A, et al. Viruses and bacteria in acute asthma exacerbations–A GA2LEN-DARE* systematic review. Allergy 2011;66:458-68.
6. Loughlin DO, Coughlan S, De Gascun C, McNally P, Cox D. The role of rhinovirus infections in young children with cystic fibrosis. Journal of Clinical Virology 2020;129:104478.
7. Mansbach JM, Piedra PA, Teach SJ, Sullivan AF, Forgey T, Clark S, et al. Prospective multicenter study of viral etiology and hospital length of stay in children with severe bronchiolitis. Archives of pediatrics & adolescent medicine 2012;166:700-6.
8. Midulla F, Pierangeli A, Cangiano G, Bonci E, Salvadei S, Scagnolari C, et al. Rhinovirus bronchiolitis and recurrent wheezing: 1-year follow-up. European Respiratory Journal 2012;39:396-402.
9. Papi A, Contoli M. Rhinovirus vaccination: the case against. Eur Respiratory Soc; 2011. p.5-7.
10. Whelan J, Fritsche K. Linoleic acid. Advances in nutrition 2013;4:311-2.
11. Marangoni F, Agostoni C, Borghi C, Catapano AL, Cena H, Ghiselli A, et al. Dietary linoleic acid and human health: Focus on cardiovascular and cardiometabolic effects. Atherosclerosis 2020;292:90-8.
12. Khoury S, Gudziol V, Grégoire S, Cabaret S, Menzel S, Martine L, et al. Lipidomic profile of human nasal mucosa and associations with circulating fatty acids and olfactory deficiency. Scientific Reports 2021;11:16771.
13. Do TQ, Moshkani S, Castillo P, Anunta S, Pogosyan A, Cheung A, et al. Lipids including cholesteryl linoleate and cholesteryl arachidonate contribute to the inherent antibacterial activity of human nasal fluid. The Journal of Immunology 2008;181:4177-87.
14. Toelzer C, Gupta K, Yadav SK, Borucu U, Davidson AD, Kavanagh Williamson M, et al. Free fatty acid binding pocket in the locked structure of SARS-CoV-2 spike protein. Science 2020;370:725-30.
15. Toelzer C, Gupta K, Yadav SK, Hodgson L, Williamson MK, Buzas D, et al. The free fatty acid–binding pocket is a conserved hallmark in pathogenic β-coronavirus spike proteins from SARS-CoV to Omicron. Science advances 2022;8:eadc9179.
16. Li C, Yang M-C, Hong P-P, Zhao X-F, Wang J-X. Metabolomic profiles in the intestine of shrimp infected by white spot syndrome virus and antiviral function of the metabolite linoleic acid in shrimp. The Journal of Immunology 2021;206:2075-87.
17. Yang S, Huang X, Li S, Wang C, Jansen CA, Savelkoul HF, et al. Linoleic acid: a natural

feed compound against porcine epidemic diarrhea disease. Journal of Virology 2023;97:e01700-23.
18. Kimura I, Ichimura A, Ohue-Kitano R, Igarashi M. Free Fatty Acid Receptors in Health and Disease. Physiological Reviews 2020;100:171-210.
19. Moonwiriyakit A, Wattanaphichet P, Chatsudthipong V, Muanprasat C. GPR40 receptor activation promotes tight junction assembly in airway epithelial cells via AMPK-dependent mechanisms. Tissue barriers 2018;6:1-12.
20. Imoto Y, Kato A, Takabayashi T, Sakashita M, Norton J, Suh L, et al. Short-chain fatty acids induce tissue plasminogen activator in airway epithelial cells via GPR 41&43. Clinical & Experimental Allergy 2018;48:544-54.
21. Antunes KH, Fachi JL, de Paula R, da Silva EF, Pral LP, Dos Santos AÁ, et al. Microbiota-derived acetate protects against respiratory syncytial virus infection through a GPR43-type 1 interferon response. Nature communications 2019;10:3273.
22. Hagihara M, Yamashita M, Ariyoshi T, Eguchi S, Minemura A, Miura D, et al. Clostridium butyricum-induced ω-3 fatty acid 18-HEPE elicits anti-influenza virus pneumonia effects through interferon-λ upregulation. Cell Reports 2022;41.
23. Antunes KH, Singanayagam A, Williams L, Faiez TS, Farias A, Jackson MM, et al. Airway-delivered short-chain fatty acid acetate boosts antiviral immunity during rhinovirus infection. Journal of Allergy and Clinical Immunology 2023;151:447-57. e5.
24. Antunes KH, Stein RT, Franceschina C, da Silva EF, de Freitas DN, Silveira J, et al. Short-chain fatty acid acetate triggers antiviral response mediated by RIG-I in cells from infants with respiratory syncytial virus bronchiolitis. EBioMedicine 2022;77.
25. Schneider WM, Chevillotte MD, Rice CM. Interferon-stimulated genes: a complex web of host defenses. Annual review of immunology 2014;32:513-45.
26. Deymier S, Louvat C, Fiorini F, Cimarelli A. ISG20: an enigmatic antiviral RNase targeting multiple viruses. FEBS Open Bio 2022;12:1096-111.
27. Zhang Y, Burke CW, Ryman KD, Klimstra WB. Identification and characterization of interferon-induced proteins that inhibit alphavirus replication. Journal of virology 2007;81:11246-55.
28. Espert L, Degols G, Gongora C, Blondel D, Williams BR, Silverman RH, et al. ISG20, a new interferon-induced RNase specific for single-stranded RNA, defines an alternative antiviral pathway against RNA genomic viruses. Journal of Biological Chemistry 2003;278:16151-8.
29. Espert L, Degols G, Lin Y-L, Vincent T, Benkirane M, Mechti N. Interferon-induced exonuclease ISG20 exhibits an antiviral activity against human immunodeficiency virus type 1. Journal of general virology 2005;86:2221-9.
30. Espert L, Rey C, Gonzalez L, Degols G, Chelbi-Alix MK, Mechti N, et al. The exonuclease ISG20 is directly induced by synthetic dsRNA via NF-κB and IRF1 activation. Oncogene 2004;23:4636-40.
31. Contoli M, Message SD, Laza-Stanca V, Edwards MR, Wark PA, Bartlett NW, et al. Role of deficient type III interferon-λ production in asthma exacerbations. Nature medicine 2006;12:1023-6.
32. Johnston SL, Papi A, Monick MM, Hunninghake GW. Rhinoviruses induce interleukin-8 mRNA and protein production in human monocytes. Journal of Infectious Diseases 1997;175:323-9.
33. Lei C, Yang J, Hu J, Sun X. On the calculation of TCID 50 for quantitation of virus infectivity. Virologica Sinica 2021;36:141-4.

34. Love MI, Huber W, Anders S. Moderated estimation of fold change and dispersion for RNA-seq data with DESeq2. Genome biology 2014;15:1-21.
35. Reich M, Liefeld T, Gould J, Lerner J, Tamayo P, Mesirov JP. GenePattern 2.0. Nature genetics 2006;38:500-1.
36. Subramanian A, Tamayo P, Mootha VK, Mukherjee S, Ebert BL, Gillette MA, et al. Gene set enrichment analysis: a knowledge-based approach for interpreting genome-wide expression profiles. Proceedings of the National Academy of Sciences 2005;102:15545-50.
37. Shim A, Song J-H, Kwon B-E, Lee J-J, Ahn J-H, Kim Y-J, et al. Therapeutic and prophylactic activity of itraconazole against human rhinovirus infection in a murine model. Scientific reports 2016;6:23110.
38. Amatore D, Celestino I, Brundu S, Galluzzi L, Coluccio P, Checconi P, et al. Glutathione increase by the n-butanoyl glutathione derivative (GSH-C4) inhibits viral replication and induces a predominant Th1 immune profile in old mice infected with influenza virus. FASEB bioAdvances 2019;1:296.
39. Goc A, Sumera W, Rath M, Niedzwiecki A. Linoleic acid binds to SARS-CoV-2 RdRp and represses replication of seasonal human coronavirus OC43. Scientific Reports 2022;12:19114.
40. Ionidis G, Hübscher J, Jack T, Becker B, Bischoff B, Todt D, et al. Development and virucidal activity of a novel alcohol-based hand disinfectant supplemented with urea and citric acid. BMC infectious diseases 2016;16:1-10.
41. Krol E, Wandzik I, Krejmer-Rabalska M, Szewczyk B. Biological evaluation of uridine derivatives of 2-deoxy sugars as potential antiviral compounds against influenza A virus. International journal of molecular sciences 2017;18:1700.
42. Arena MP, Capozzi V, Russo P, Drider D, Spano G, Fiocco D. Immunobiosis and probiosis: antimicrobial activity of lactic acid bacteria with a focus on their antiviral and antifungal properties. Applied microbiology and biotechnology 2018;102:9949-58.
43. Barnard KN, Alford-Lawrence BK, Buchholz DW, Wasik BR, LaClair JR, Yu H, et al. The effects of modified sialic acids on mucus and erythrocytes on influenza A virus HA and NA functions. bioRxiv 2019:800300.
44. Fonseca W, Malinczak C-A, Schuler CF, Best SK, Rasky AJ, Morris SB, et al. Uric acid pathway activation during respiratory virus infection promotes Th2 immune response via innate cytokine production and ILC2 accumulation. Mucosal Immunology 2020;13:691-701.
45. Jiao J, Meng N, Wang H, Zhang L. The effects of vitamins C and B12 on human nasal ciliary beat frequency. BMC Complementary and Alternative Medicine 2013;13:1-6.
46. Martens K, Pugin B, De Boeck I, Spacova I, Steelant B, Seys S, et al. Probiotics for the airways: potential to improve epithelial and immune homeostasis. Allergy 2018;73:1954-63.
47. Polonikov A. Endogenous deficiency of glutathione as the most likely cause of serious manifestations and death in COVID-19 patients. ACS infectious diseases 2020;6:1558-62.
48. Ran L, Zhao W, Wang J, Wang H, Zhao Y, Tseng Y, et al. Extra dose of vitamin C based on a daily supplementation shortens the common cold: A meta-analysis of 9 randomized controlled trials. BioMed research international 2018;2018.
49. Silvagno F, Vernone A, Pescarmona GP. The role of glutathione in protecting against the severe inflammatory response triggered by COVID-19. Antioxidants 2020;9:624.
50. Müller M, Stefanetti F, Krieger UK. Oxidation pathways of linoleic acid revisited with electrodynamic balance–mass spectrometry. Environmental Science: Atmospheres

2023;3:85-96.
51. Fujisawa S, Kadoma Y, Yokoe I. Radical-scavenging activity of butylated hydroxytoluene (BHT) and its metabolites. Chemistry and physics of lipids 2004;130:189-95.
52. Malamud D, Abrams W, Barber C, Weissman D, Rehtanz M, Golub E. Antiviral activities in human saliva. Advances in dental research 2011;23:34-7.
53. Müller H, End C, Weiss C, Renner M, Bhandiwad A, Helmke B, et al. Respiratory Deleted in Malignant Brain Tumours 1 (DMBT1) levels increase during lung maturation and infection. Clinical & Experimental Immunology 2008;151:123-9.
54. Stoddard E, Cannon G, Ni H, Karikó K, Capodici J, Malamud D, et al. gp340 expressed on human genital epithelia binds HIV-1 envelope protein and facilitates viral transmission. The Journal of Immunology 2007;179:3126-32.
55. Furutani Y, Toguchi M, Higuchi S, Yanaka K, Gailhouste L, Qin X-Y, et al. Establishment of a rapid detection system for ISG20-dependent SARS-CoV-2 subreplicon RNA degradation induced by interferon-α. International Journal of Molecular Sciences 2021;22:11641.
56. Bochkov YA, Busse WW, Brockman-Schneider RA, Evans MD, Jarjour NN, McCrae C, et al. Budesonide and formoterol effects on rhinovirus replication and epithelial cell cytokine responses. Respiratory research 2013;14:1-9.
57. Spurrell JC, Wiehler S, Zaheer RS, Sanders SP, Proud D. Human airway epithelial cells produce IP-10 (CXCL10) in vitro and in vivo upon rhinovirus infection. American Journal of Physiology-Lung Cellular and Molecular Physiology 2005;289:L85-L95.
58. Zaheer R, Wiehler S, Hudy M, Traves S, Pelikan J, Leigh R, et al. Human rhinovirus-induced ISG15 selectively modulates epithelial antiviral immunity. Mucosal immunology 2014;7:1127-38.
59. Alsabeeh N, Chausse B, Kakimoto PA, Kowaltowski AJ, Shirihai O. Cell culture models of fatty acid overload: Problems and solutions. Biochimica et Biophysica Acta (BBA)-Molecular and Cell Biology of Lipids 2018;1863:143-51.
60. Gonçalves de Albuquerque CF, Burth P, Younes Ibrahim M, Garcia DG, Bozza PT, Castro Faria Neto HC, et al. Reduced plasma nonesterified fatty acid levels and the advent of an acute lung injury in mice after intravenous or enteral oleic acid administration. Mediators of Inflammation 2012;2012:601032.
61. Naughten S, Ecklu-Mensah G, Constantino G, Quaranta A, Escalante KS, Bai-Tong S, et al. The re-emerging role of linoleic acid in paediatric asthma. European Respiratory Review 2023;32.
62. Tang HH, Lang A, Teo SM, Judd LM, Gangnon R, Evans MD, et al. Developmental patterns in the nasopharyngeal microbiome during infancy are associated with asthma risk. Journal of Allergy and Clinical Immunology 2021;147:1683-91.
63. Kloepfer KM, Sarsani VK, Poroyko V, Lee WM, Pappas TE, Kang T, et al. Community-acquired rhinovirus infection is associated with changes in the airway microbiome. Journal of Allergy and Clinical Immunology 2017;140:312-5. e8.
64. Rosas-Salazar C, Shilts MH, Tovchigrechko A, Chappell JD, Larkin EK, Nelson KE, et al. Nasopharyngeal microbiome in respiratory syncytial virus resembles profile associated with increased childhood asthma risk. American journal of respiratory and critical care medicine 2016;193:1180-3.
65. Bomar L, Brugger SD, Yost BH, Davies SS, Lemon KP. Corynebacterium accolens releases antipneumococcal free fatty acids from human nostril and skin surface triacylglycerols. MBio 2016;7:10.1128/mbio. 01725-15.

66. Szabo D, Ostorhazi E, Stercz B, Makra N, Penzes K, Kristof K, et al. Specific nasopharyngeal Corynebacterium strains serve as gatekeepers against SARS-CoV-2 infection. Geroscience 2023;45:2927-38.
67. Husted AS, Trauelsen M, Rudenko O, Hjorth SA, Schwartz TW. GPCR-mediated signaling of metabolites. Cell metabolism 2017;25:777-96.
68. Moonwiriyakit A, Wattanaphichet P, Muanprasat C. GPR40 promotes tight junction assembly in human airway epithelial cells via AMPK-dependent mechanisms. Eur Respiratory Soc; 2018.
69. Lee K-P, Park S-J, Kang S, Koh J-M, Sato K, Chung H-Y, et al. ω-3 Polyunsaturated fatty acids accelerate airway repair by activating FFA4 in club cells. American Journal of Physiology-Lung Cellular and Molecular Physiology 2017;312:L835-L44.
70. Prihandoko R, Kaur D, Wiegman CH, Alvarez-Curto E, Donovan C, Chachi L, et al. Pathophysiological regulation of lung function by the free fatty acid receptor FFA4. Science translational medicine 2020;12:eaaw9009.
71. Moonwiriyakit A, Yimnual C, Noitem R, Dinsuwannakol S, Sontikun J, Kaewin S, et al. GPR120/FFAR4 stimulation attenuates airway remodeling and suppresses IL-4-and IL-13-induced airway epithelial injury via inhibition of STAT6 and Akt. Biomedicine & Pharmacotherapy 2023;168:115774.
72. Kuperman DA, Huang X, Koth LL, Chang GH, Dolganov GM, Zhu Z, et al. Direct effects of interleukin-13 on epithelial cells cause airway hyperreactivity and mucus overproduction in asthma. Nature medicine 2002;8:885-9.
73. Nelson RK, Bush A, Stokes J, Nair P, Akuthota P. Eosinophilic asthma. The Journal of Allergy and Clinical Immunology: In Practice 2020;8:465-73.
74. Hammad H, Lambrecht BN. The basic immunology of asthma. Cell 2021;184:1469-85.
75. White MR, Crouch E, Van Eijk M, Hartshorn M, Pemberton L, Tornoe I, et al. Cooperative anti-influenza activities of respiratory innate immune proteins and neuraminidase inhibitor. American Journal of Physiology-Lung Cellular and Molecular Physiology 2005;288:L831-L40.
76. Madsen J, Tornøe I, Nielsen O, Lausen M, Krebs I, Mollenhauer J, et al. CRP-ductin, the mouse homologue of gp-340/deleted in malignant brain tumors 1 (DMBT1), binds gram-positive and gram-negative bacteria and interacts with lung surfactant protein D. European journal of immunology 2003;33:2327-36.
77. Liu Y, Nie H, Mao R, Mitra B, Cai D, Yan R, et al. Interferon-inducible ribonuclease ISG20 inhibits hepatitis B virus replication through directly binding to the epsilon stem-loop structure of viral RNA. PLoS pathogens 2017;13:e1006296.
78. Leong CR, Funami K, Oshiumi H, Mengao D, Takaki H, Matsumoto M, et al. Interferon-stimulated gene of 20 kDa protein (ISG20) degrades RNA of hepatitis B virus to impede the replication of HBV in vitro and in vivo. Oncotarget 2016;7:68179.
79. Stadler D, Kächele M, Jones AN, Hess J, Urban C, Schneider J, et al. Interferon-induced degradation of the persistent hepatitis B virus cccDNA form depends on ISG20. EMBO reports 2021;22:e49568.
80. Hoopes JI, Cortez LM, Mertz TM, Malc EP, Mieczkowski PA, Roberts SA. APOBEC3A and APOBEC3B preferentially deaminate the lagging strand template during DNA replication. Cell reports 2016;14:1273-82.
81. Diamond MS, Farzan M. The broad-spectrum antiviral functions of IFIT and IFITM proteins. Nature Reviews Immunology 2013;13:46-57.
82. Wu N, Nguyen X-N, Wang L, Appourchaux R, Zhang C, Panthu B, et al. The interferon

stimulated gene 20 protein (ISG20) is an innate defense antiviral factor that discriminates self versus non-self translation. PLoS pathogens 2019;15:e1008093.

83. Agus A, Clément K, Sokol H. Gut microbiota-derived metabolites as central regulators in metabolic disorders. Gut 2021;70:1174-82.

84. Mercola J, D'Adamo CR. Linoleic acid: a narrative review of the effects of increased intake in the standard American diet and associations with chronic disease. Nutrients 2023;15:3129.

Abstract in Korean

리노바이러스 감염 시 리놀레산의 항바이러스 효과 및 조절 기전

리노바이러스(HRV) 감염은 일반적인 감기를 비롯하여 중이염, 천식 악화, 기관지염 등 다양한 호흡기 질환과 관련되어 있습니다. 그러나 현재까지 HRV 감염에 대한 특이적인 치료제나 백신은 개발되지 않았기 때문에, 이러한 치료제 및 백신 개발을 위한 연구가 절실히 요구됩니다. 본 연구에서는 리놀레산(LA)이 HRV 감염을 억제하는 데 기여할 수 있음을 제시합니다.

우선, 인간 비강 세척액을 이용하여 역전사 실시간 중합효소 연쇄반응(RT-qPCR)을 통해 HRV 양성군(n = 6)과 음성군(n = 9)으로 구분한 후, 표적 질량분석을 통해 두 군 간의 차이를 보이는 대사체를 분석했습니다. 그 결과, HRV 양성군에서 유의하게 증가한 리놀레산(LA)이 기도 상피 세포에서 HRV 감염을 억제하는 효과를 나타냄을 관찰했습니다.

세포 실험을 통해 LA의 항바이러스 효과가 LA의 수용체로 알려진 G-단백질 결합 수용체(GPR)40 및 GPR120에 의존적임을 길항제 처리 실험을 통해 입증했습니다. 또한, 염기서열 분석 결과 LA 처리에 의해 항바이러스 단백질인 인터페론 자극 유전자 20 kDa(ISG20)의 발현이 유도됨을 확인했고, ISG20의 발현을 억제할 경우 LA의 항바이러스 효과가 상실되는 것을 기도 상피 세포 실험에서 관찰했습니다. 이는 LA의 항바이러스 작용이 ISG20에 의해 매개됨을 시사합니다.

아울러, NF-κB 억제 실험을 통해 ISG20의 발현이 LA에 의해 활성화되는 NF-κB 신호 경로와 관련되어 있음을 관찰했습니다. 마우스 모델에서도 LA가 비강을 통해 기도 상피에 전달될 수 있으며, 생체 내에서도 GPR40/120 의존적으로 HRV 복제를 억제하고 병리적 염증 반응을 완화하는 효과를 나타냄을 확인했습니다.

종합적으로, 본 연구는 GPR40/120와 ISG20, NF-κB를 통해 작용하는 LA의 항바이러스 효과를 규명했으며, LA가 HRV 감염과 관련된 다양한 호흡기 질환을 완화하는 치료 후보물질로 활용될 수 있음을 제시합니다.

핵심되는 말 : 리노바이러스, 리놀레산 (LA), 인터페론 자극 유전자 20kDa (ISG20), 핵인자 카파비 B(NF-κB), G-단백질 결합 수용체 40/120, 항바이러스 효과